NASA CR-54760

DEVELOPMENT OF IMPROVED SINGLE CRYSTAL

GALLIUM PHOSPHIDE SOLAR CELLS

Final Report

15 August, 1964 - 15 August, 1965

Contract No. NAS3-6014

Placed by

NATIONAL AERONAUTICS AND SPACE ADMINSTRATION

Lewis Research Center

Cleveland, Ohio

MONSANTO RESEARCH CORPORATION

A SUBSIDIARY OF MONSANTO COMPANY

DAYTON

LABORATORY

DAYTON, OHIO 45407

DEVELOPMENT OF IMPROVED SINGLE CRYSTAL

GALLIUM PHOSPHIDE SOLAR CELLS

Final Report
15 August, 1964 - 15 August, 1965

Contract No. NAS3-6014

NATIONAL AERONAUTICS AND SPACE ADMINISTRATION
Technical Management
Space Power Systems Division
NASA Lewis Research Center
Attention: L. R. Scudder

Report Prepared by: W. O. Groves and A. S. Epstein

Edited by: R. A. Ruehrwein

Work Performed by:
Central Research Department
Monsanto Company, Saint Louis, Missouri

Requests for copies of this report should be referred to:

National Aeronautics and Space Administration
Office of Scientific and Technical Information
Washington, D. C.   20025
Attn: AFSS-A

NOTICE

TABLE OF CONTENTS

I.   PURPOSE

This is the final report on the development of gallium phosphide solar cells under this contract, a continuation of the program initiated in June, 1963.

The objective of this program was the development of an efficient solar cell operable at temperatures up to 500° C, with major emphasis on improvement of the gallium phosphide material. The approach was to grow single crystal gallium phosphide by epitaxial deposition from the vapor phase on gallium arsenide substrate, followed by removal of the gallium arsenide. Diffused junction cells were then fabricated and the photovoltaic properties of the cells were measured up to high temperatures. The design and performance of the cells was related to the electrical and optical properties of the gallium phosphide.

II.   ABSTRACT

Single crystal gallium phosphide has been prepared by vapor deposition on gallium arsenide substrates in the open tube system, using several different methods for generating the reaction gas mixture in a search for higher purity reactants. Sources for the transport gas investigated have included PCl_3, $AsCl_3$, trichloroethylene and water vapor. Sources for phosphorus have included elemental phosphorus, PCl_3, GaP, PH_3, and P_3N_5. Thick, self-supporting crystals have been grown over a wide range of temperatures and flow conditions. Most, however, in order to maximize purity, have been grown at low temperatures and low growth rates.

$GaAs_{(1-x)}P_x$ alloy single crystals have been prepared in the same system using elemental gallium and phosphorus with $AsCl_3$ as the source of arsenic and transport agent.

Improved electrical properties, lower net carrier concentrations and higher mobility, obtained with the chloride transport systems have indicated a significant improvement in purity over earlier results. Quantitative analyses of single crystal GaP samples by emission spectroscopy and analysis of electrical measurements as a function of temperature indicate total ionized impurity concentrations as low as 3×10^{16} cm^{-3}.

A pronounced effect of orientation on segregation of impurities and dopants has again been observed and extended to include <211> orientations. With the improvement in purity, the best orientation, in terms of solar cell performance, is the <111>B.

Water vapor grown crystals, except those intentionally doped with tellurium, have all had very high resistivities. The oxygen doping appears to have an adverse effect on the open circuit voltage of solar cells.

Tellurium doping, as a method for upgrading solar cell performance of normally high resistivity material, has been successful

only in the case of a water vapor grown crystal doped in the low 10^{16} cm^{-3} range. A high degree of compensation and a large segregation with orientation have been shown by electrical and chemical analyses of heavily Sn doped crystals.

Effects of the transport system used on the structural perfection of the crystals have been observed. The effect of lattice mismatch and thermal expansion difference of GaP and GaAs on dislocation and strain in the crystals have been discussed and the structure of several crystals examined by strain birefringence observation and dislocation etching. Structural imperfections may have a strong influence on the formation and behavior of p-n junctions.

A close-space water vapor transport technique for growing single crystal GaP has been investigated briefly. Thick self-supporting layers have been grown but the structure has been poor and alloying with the GaAs substrate has been extensive. The requirement of a presynthesized GaP source makes this technique less attractive than the open tube system on the basis of purity and flexibility.

The best GaP solar cells fabricated from the high purity material have had conversion efficiencies of almost 2% in sunlight at room temperature with open circuit voltages of 1.40 volts and short circuit currents of 1.6 ma/cm^2; at 350° C, the best open circuit voltage was 0.45 volts.

At higher solar intensities, there is evidence that the GaP solar cell conversion efficiencies increase to better than 3.5%. This suggests that with further improvement in fabrication techniques and material control and purity, considerable improvement in the conversion efficiency and solar cell properties can be expected at solar intensities (80-90 mw/cm^2) normally used for testing.

At present an upper temperature limit of 350° C has been found for the GaP solar cell. This limitation is imposed because of the use of zinc as a diffusant and difficulty in finding good contacts

above 350° C. As fabrication techniques are improved this temperature limitation will be lifted.

Preliminary work with GaAsP has shown that at high solar intensities, for a composition $GaAs_{.43}P_{.57}$ solar cells of 5% conversion efficiency can be achieved.

III.   MATERIAL PREPARATION

A.   INTRODUCTION

The objective of the material preparation program, continuing the work of the previous contract[1], has been to determine the requirements for preparing high quality single crystal gallium phosphide--this material subsequently to be used in a critical evaluation of the potential of gallium phosphide in high temperature solar cells. The material objectives have been to prepare single crystals of at least 1 cm^2 area, thick enough for self support, and free of gross defects such as bumps, stacking faults, and polycrystalline grain boundaries; and of as high purity as possible based on electrical and analytical measurements.

Based on the earlier work[1], the methods for crystal growth to be investigated were:

(1) Epitaxial growth of gallium phosphide on gallium arsenide substrates by the open tube, hydrogen chloride transport process. Steps to be taken to improve the purity of the gallium phosphide were to include the use of tube liners such as alumina in the reactor to reduce silicon contamination, and the use of higher purity sources of phosphorus and hydrogen chloride.

(2) Epitaxial growth by the open tube water vapor transport process, establishing whether or not oxygen doping can be tolerated.

(3) Epitaxial growth by a close-space process using water vapor or other suitable transport agent.

In addition, the best substrate face orientation and the effects of doping with both n- and p-type dopants were to be investigated.

B.   OPEN TUBE TRANSPORT PROCESSES

Earlier work[1] had shown that thick, self supporting single crystals of GaP could be grown by epitaxial deposition on single crystal GaAs in an open tube system using HCl transport. Although this system

appeared to place definite limitations on growth rates and yields, it did have the advantage of permitting direct synthesis from the elements at relatively low temperatures, and so offered the most promising route to high purity GaP. The similar system using H_2O transport showed promise of higher growth rates and yields and improved structure. In addition, even though higher temperatures are required, improved purity (except for oxygen contamination) might result from oxygen suppression of reaction with silica and from the fact that the oxides of most elements are much less volatile than the corresponding chlorides.

Since a primary objective of the program has been to improve purity of the GaP, these systems have been investigated most extensively. Details of the experimental procedure may be found in reference (1) and in previous quarterly reports[2, 3, 4].

In the search for higher purity, several different sources of raw materials--for transport agent, phosphorus and gallium--have been investigated. A skeleton outline of the various combinations employed is presented in Table I. The reagents were the highest purity commercially available; their source is also listed in Table I.

The chloride systems listed (possibly excepting that using trichloroethylene, a novel source of transport agent) involve basically the same chemical reactions. Hydrogen chloride is generated by hydrogen reduction of the transport agent source at high temperature; carried out in a separate furnace in the case of $AsCl_3$ and C_2HCl_3 to permit subsequent removal of arsenic and carbon. In the latter case, the amount of carbon deposited accounted for only a small portion of the trichloroethylene, but the amount of gallium transported per chlorine equivalent, and yields of GaP obtained, were the same as with the other chloride transport agent sources under equivalent flow and temperature conditions. The gallium sources are saturated with phosphorus and covered with a crust of GaP during the start up and pretreatment period.
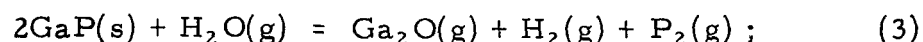
The basic chemical reactions, therefore, are: at the source,

$$GaP(s) + HCl(g) = GaCl(g) + \tfrac{1}{2}H_2(g) + \tfrac{1}{2}P_2(g) ; \qquad (1)$$
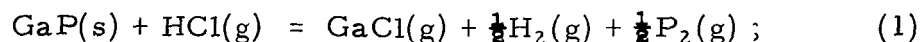
and in the deposition zone, reversal of (1) and the disproportionation,

$$3GaCl(g) + P_2(g) = 2GaP(s) + GaCl_3(g) . \qquad (2)$$
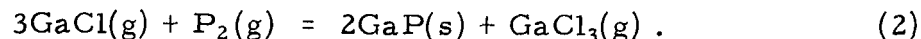
The reactions in the water vapor systems are analagous to (1),

$$2GaP(s) + H_2O(g) = Ga_2O(g) + H_2(g) + P_2(g) ; \qquad (3)$$

the forward reaction taking place at the source, the reverse in the deposition zone[5]. In the run in which P_3N_5 was used as a phosphorus source, transport of GaP was normal but the nitrogen evolved nitrided the GaAs substrates and destroyed the surface for nucleation of GaP.

The principal differences between the chloride and oxide transport systems are in the temperature range covered by the reaction and the region of the reaction range usable for single crystal growth. The chloride transport reactions occur at much the lower temperatures and the requirements for single crystal growth necessitate operating at the upper end of the range. Thus, at the source temperature, the atom ratio of gallium transported to chlorine introduced approaches unity. The gallium to chlorine ratio at the minimum deposition temperature for single crystal growth is still fairly high, that is, most of the GaP deposition occurs at lower temperatures where only poly- crystalline growth can be obtained. Source temperatures have normally been about 900° C with deposition temperatures for single crystal growth ranging from about 870° to 800° C at initial HCl pressures of the order of 2-5 x 10^{-3} atm. The reaction can be shifted to higher temperatures by increasing the initial HCl pressure but at the higher deposition rates the minimum deposition temperature for single crystal growth is also increased and yields obtained remain low. For example, with an initial HCl pressure of about 0.1 atm and a source temperature of 1000° C,

the minimun deposition temperature for single crystal growth is about 900° C.

In contrast, the water vapor transport reactions occur at high temperatures (1100° C source) and single crystal growth can be obtained at even the low end of the reaction range. It is advantageous to use low initial H_2O pressures to shift the reaction to lower temperatures thus minimizing contamination by reaction with quartz.

In all of these systems, with suitable choice of growth orientation, the material objectives of area, thickness, and structural perfection have been demonstrated. The PCl_3[2, 3] and trichloroethylene[4] systems have been investigated over a wide range of temperature and flow conditions. Electrical properties and solar cell characteristics of material grown using PCl_3 contained trends indicating increasing contamination with increase in source temperature. Most runs, therefore, including all those employing $AsCl_3$, have been made under low temperature (source at $\sim 900°$) conditions requiring slow growth rates to maximize purity. Recent solar cell data (Table IX) and electrical measurements[4] of trichloroethylene grown material, however, have not shown such trends with source temperature and so improved structure and/or higher growth rates might be attained at higher temperatures without sacrificing purity.

With the improvement in purity achieved using these chloride transport agent sources, the <111>B grown crystals have shown the best solar cell characteristics. Therefore, recent efforts have been directed towards increasing the yield of crystals of this orientation. Conditions and yields of recent runs are summarized in Table II.

The results of the first and last three runs show that high yields (>25%) are possible in both the trichloroethylene and $AsCl_3$ transport systems. A similar result had been obtained previously in the PCl_3 system (Run SC65, Table I, Ref. (3)). The determining factor under these flow and temperature conditions is the number

(or total surface area) and position of the substrate wafers. In all of these runs the wafers were supported vertically, parallel to the gas flow and virtually all GaP deposition within the substrate zone took place on the wafers. Since much of the deposition occurs on the <111>A side and leading edges of wafers so supported, the yield of <111>B growth is considerably lower, but <111>B crystals of 0.2-0.4 mm in thickness and nearly free of polycrystalline nodules were obtained.

In Run SC92 an attempt was made to increase the yield and thickness uniformity of <111>B grown crystals by supporting the wafers on plates at 30° to the horizontal. Polycrystallinity resulted, due either to the increased deposition rate or to poor control at the start of the run. However, there was also a pronounced thickness gradient from front to back. Pyrolytic BN, used for the support plate, has a very high thermal conductivity parallel to the substrate surface[6] which effectively reduces the temperature gradient. The gas flow pattern established past the support system may also have been a contributing factor.

To increase the yield of <111>B crystal, in Run SC94, at each position, two <111> wafers were placed back to back. Heavy polycrystalline growth at the edges of the wafers limited the thickness attained to 0.2-0.3 mm and breakage prevented recovery of most large area pieces but the technique does show some promise.

Phosphine, as a 1% mixture in hydrogen, was used successfully as the source of phosphorus in two runs, SC93 and AP139.

Single crystal $GaAs_{(1-x)}P_x$ alloys were grown (Run SC91) using high purity $AsCl_3$ and elemental phosphorus as the sources of arsenic and phosphorus. The $AsCl_3$ vapor (in H_2) at a controlled rate was passed directly into the furnace system without prior reduction and the phosphorus temperature controlled to give the desired P/(P + As) atom ratio in the vapor. Both <100> and <111>B crystals were grown. Growth rates and yields were in line with those of GaP crystals grown

under similar conditions. X-ray analyses of top and bottom surfaces and electron microprobe analysis of the profile from a cleaved section of the <100> wafer indicated composition uniformity within less than 2%. A small, but significant, difference in composition was found for adjacent crystals of different orientation. With a P/(P + As) atom ratio of 0.495 in the vapor, the composition of the <100> deposits was 60.5 mole % GaP; that of the <111>B, 56.5%.

In the water vapor transport system yields and growth rates were generally higher (Table IV, Ref. (3))) than in the chloride system with horizontally supported substrates and could probably have been increased further with vertically supported substrates. Yields, as has been mentioned, are potentially higher in the water vapor system than in the chloride systems.

C. ELECTRICAL PROPERTIES

Typical electrical properties of undoped GaP single crystals grown on different substrate orientations using the different systems are summarized in Table III. Data from the earlier work using an HCl source[1] are included for comparison. Values for resistivity and net carrier concentrations may vary over an order of magnitude; where the range is greater, this has been indicated. Except for the samples grown at a higher temperature and growth rate using PCl_3 , it is evident, from the reduction in net carrier concentrations and increase in mobilities, that the new chloride transport agent sources have led to a significant increase in purity over that obtained with the earlier HCl source. There is not, however, with the same exception, a significant difference among the three chloride sources evident from the elctrical data.

The results of the high temperature, high growth rate run using trichloroethylene, showing an apparent improvement in electrical properties, suggest that a mechanism other than an increased attack on

quartz is responsible for the degradiation of electrical properties in the high temperature PCl_3 runs.

The pronounced effect of orientation on electrical properties due to differences in segregation coefficients of impurities[1] is apparent in all of the chloride transported material, the data being extended to include <211> orientations. The <211> orientations are designated A and B corresponding to the nearest <111> orientation. It is interesting to note that segregation effects on the <211> orientations are similar to those on the corresponding <111> orientations. The apparent order of decreasing net carrier level is <111>B > <211>B > <110> > <100> > <111>A, <211>A. Growth on the last three orientations using PCl_3, $AsCl_3$, or trichloroethylene has usually produced material of high resistivity.

All undoped GaP, irrespective of orientation, produced by water vapor transport has been of high resistivity; probably due to suppression of shallow donor impurities, such as silicon, and overwhelming compensation of shallow acceptors by the deep donor levels introduced by oxygen.

While significant differences in electrical properties due to impurity differences are not apparent among the different chloride transport systems, this is not true of certain structural and growth characteristics, discussed in a later section, or of solar cell performance.

The best solar cell performance has been obtained in <111>B crystals (NA68 SC76-4 and NA68 SC77-4, Tables IX and X, Ref. (4)) grown at low temperature and low growth rate in quartz, using $AsCl_3$ as the transport agent source. Good performance has also been found in trichloroethylene grown GaP (NA69 SC86-2<111>B, Table IX, Ref. (4), and Table IX of this report). Because of its high resistivity, solar cell performance of undoped water vapor grown GaP has been poor, but it has been possible to upgrade the performance by tellurium doping as will be discussed in the next section.

The best PCl$_3$ grown GaP, while not differing appreciably in electrical properties and having excellent diode characteristics, showed definitely inferior solar cell characteristics, V_{oc}'s being down by 0.1 volt and more at both room temperature and 350°. Furthermore, the short circuit currents tended to degrade on heating to 350° C[3].

The main effect on electrical properties of a BN tube liner, introduced in an attempt to reduce silicon contamination, was to produce a high degree of uniformity along the deposition zone, in contrast to the usual large segregation effect encountered. Inferior characteristics and abnormal spectral response of solar cells, however, indicated an increase in contamination introduced by the BN.

Electrical data for individual crystals from recent runs are listed in Table IV. Also shown are the approximate deposition temperatures. The electrical properties of the first four runs listed are similar to those previously obtained and discussed above. The low mobilities measured in the SC92 samples is probably due to the high degree of polycrystallinity.

Electrical properties of the GaAs$_{(1-x)}$P$_x$ alloy crystals produced in Run SC91 are similar to those found for GaP except for the lower mobility, probably due to the alloy composition. Solar cell performance of both samples, interestingly, was as good (Table X) as some of the better GaP samples, open circuit voltages at both room temperature and 350° C being much closer to the theoretical values for these compositions.

D.   DOPING

Some tellurium doping experiments, as described in earlier reports[1,3,4], were carried out in an attempt to upgrade normally high resistivity material, and so obtain a more valid evaluation of solar cell potential. Tellurium doped material was also produced in two runs in which a doped GaP source was used. Recently, in a preliminary run

(AP139, Table II) to explore conditions for tin doping vapor grown GaP, very heavily tin toped GaP crystals of several orientations have been obtained. The data are summarized in Table V.

As may have been expected from the previously observed effect of orientation on net carrier level, the ratio of gas dopant concentration to net carrier level is much higher for the <111>A and <100> orientation than for the <111>B. The relatively high carrier level obtained in Run SC72 for <100> growth using water vapor transport must be attributed to the high water vapor pressure used although the orientation effects may not be as great in this system as in the chloride transport system.

Only in samples of Run SC73 were good electrical properties (high mobilities, moderate carrier concentrations) obtained, and only in these samples was good solar cell performance observed. Open circuit voltages, even of these samples, however, were low. The poor solar cell performance and abnormal spectral response of the SC87 samples, although having excellent structure and doped to the optimum range, must have been due to unidentified contamination introduced by the BN tube liner.

In the electrical data for the samples of Run AP139, the effect of orientation on dopant concentration is not shown by the net carrier concentration but is clearly evident in the mobilities. It was also clearly evident in the color of the crystals which ranged from a slight darkening of the <100> and <111>A to virtual nontransparency of the <111>B. Spectroscopic emission analyses revealed 130 ppm and 150 ppm Sn for AP139-6<100> and AP139-3<111>A, respectively, and greater than 800 ppm for AP139-3<111>B. These correspond to 2.7×10^{18}, 3.2×10^{18}, and $\sim 1.8 \times 10^{19}$ atoms/cm^3 respectively. Thus the high degree of compensation, expected because of the amphoteric nature of Sn in GaP, is evident.

The order of decreasing dopant concentrations for Sn, based

on the electrical and analytical data, and supported by observation of color, is slightly different than that deduced earlier for net carrier levels produced by unintentional impurities. This is <111>B > <211>B > <211>A > <111>A , <100>.

A striking example of inhomogeneity that can be produced in a growing crystal with non planar defects by the orientation segregation effect is provided in Figure 1. This is a slightly enlarged photograph of a <100> crystal, AP139-5, polished on both sides, taken with diffused transmitted light. The sample originally contained broad, flat topped bumps of the rounded rectangular type. The dark regions are regions of high Sn concentration produced because the actual growth surfaces on opposite sides of each bump were close to the <111>B orientations. The small very dark spots are thin twinned regions where the twinning has brought a <111>B direction close to the actual growth direction.

E. EMISSION SPECTROSCOPIC ANALYSIS

In the last quarterly report[4] results of quantitative analyses of selected samples of epitaxially grown single crystal GaP were given and correlation of these results with electrical properties and solar cell characteristics attempted. More recent analyses of additional samples, some from the same runs as those reported previously, show impurity concentrations lower by an order of magnitude or more. Since the major source of error in the analytical technique is extraneous contamination of the sample, the lower values must be considered more valid. The latest analyses are tabulated in Table VI.

The impurity concentrations reported are generally in the low 10^{16} cm^{-3} range or less. This is in agreement with the analysis of electrical measurements as a function of temperature discussed in section IV, B. below. It is concluded, therefore, that the purity of the vapor grown GaP crystals is appreciably higher than has been heretofore assumed.

Agreement between silicon analyses and net carrier concentrations within a factor of two is found in eight of the fourteen samples. In all of the exceptions, save one, the silicon analysis is higher and might therefore be spurious. In SC90-6, in which silicon is lower, the main donor impurity is probably sulfur, as discussed in section IV, B. below. Corollary to this relationship, the dependence of net carrier concentration on orientation appears to be due to the segregation of silicon.

Identification of the impurity or impurities responsible for the limitations on the characteristics of GaP solar cells on the basis of these analyses is not possible. Silicon (as in SC76-4<111>B) appears to be a suitable dopant to provide the necessary n-type conductivity and there is no correlation with Ca or Mg concentrations.

F.   STRUCTURE

Surface defects and the factors causing them have been discussed in some detail earlier[1] and during the current work additional observations have been made[2, 3, 4]. Recently, investigation of structural imperfections by strain birefringence and dislocation etch techniques has been initiated.

1.   Effect of Transport System on Structure

Although, as discussed above, the chemistry involved in the various transport systems is basically the same, and closely similar electrical properties have been obtained, there is an effect of the different chloride transport systems on the structure of the GaP crystal. This effect is reflected in the ease with which good structure (freedom from bumps, stacking faults and polycrystallinity) can be obtained as well as in the preferred growth orientation. These must in turn reflect differences in impurities and impurity concentrations in the transport gas mixture and in the growing crystal. The water vapor transport systems are excluded from this discussion because of the great difference

in conditions as well as in chemistry involved. In one run, however, using a high initial water vapor pressure and Te doping, the <100> growth surface defects strongly resembled those seen in chloride transport systems.

In the chloride transport systems good structure can be obtained by shifting to higher deposition temperatures or to lower initial HCl pressures and lower growth rates. On this basis the requirements for growing good surfaces are most stringent in the PCl_3 system. At the same time, <111>B surfaces of PCl_3 transported GaP are much superior to the <100>. Although containing many features, such as growth steps and triangular mesas, (Figure 26, Ref. (3)), <111>B surfaces are generally free of the polycrystalline nodules found on <111>B surfaces of crystals grown using the other chloride systems. In contrast, the $AsCl_3$ system produces excellent <100> surfaces while tending to allow formation of polycrystalline nodules on the <111>B. Direct evidence that this may be an impurity effect is found in the tellurium doping experiments using $AsCl_3$ transport in which polycrystallinity on the <111>B surface was extreme. The trichloroethylene system is equivalent to the $AsCl_3$ system with perhaps less tendency toward polycrystallinity on the <111>B.

Typical <100>, <111>A, <111>B, and <110> surfaces have been shown in previous reports. In Figure 2, typical <211>A and <211>B oriented crystals grown using the trichloroethylene or $AsCl_3$ transport systems are illustrated. Enlarged views of the same surfaces are shown in Figure 3. The <211>B surfaces are rough with numerous pits, some very deep. The structure of the <211>A surfaces may be related to the faceted pits which develop on <111>A surfaces (Figure 2a, Ref. (3)). The radical effect on the surface appearance produced by heavy tin doping is illustrated in Figure 4.

2.   Dislocations and Strain

Lattice mismatch of GaP and GaAs, since the crystals are

grown at temperatures in the plastic deformation region, may be expected to produce dislocations in the interface region, rather than a high degree of strain. Strain, not relieved by generation of dislocations, should be produced by the thermal expansion difference as the wafer cools rapidly from the deposition temperatures. The GaAs substrate, with a thick GaP deposit on each side, will come under tension. With the additional stress applied by the handling necessary to grind off the edge deposit, the substrate usually cracks along cleavage planes perpendicular to the surface. The cracks extend a short distance into the GaP layers on each side also, so that on etching the substrate out, patterns of grooves which are mirror images appear on the two GaP crystals. This mechanism may also account for the cleavage pattern shown in Figure 5. The built-in strain prevents application of the uniform stress necessary to produce smooth cleavage across the whole cross section of the wafer.

The region of mismatch dislocations and strain in the GaP crystal, however, should be close to the substrate interface and be removed with the substrate on etching in warm nitric acid. (Any alloyed region will also be removed.) Therefore, the strain remaining in the crystal after substrate removal must arise from another mechanism.

Such additional strain has been observed, in four samples grown on four different orientations, as birefringence under crossed polarizers in the microscope. Some typical results are shown in Figures 6 through 9. Contrary to the results reported by Gershenzon and Mikulyak[7] on annealing of GaP grown by water vapor transport, the strain was not removed by annealing at 980° for 26 hours. However, the strain in these crystals, for the most part as will be shown, seems to be associated with stacking fault arrays and locked dislocations, defects which are probably built into the growing crystal.

The structure of the four crystals shown in Figures 6 through

9 has been examined by selective etching.

<u><111>A</u> . The stacking fault structure of the <111>A grown crystal (C_2HCl_3 , P , Ga , low temp.), whose strain birefringence pattern is shown in Figure 6, is shown in Figure 10. This was developed by etching for approximately 3 hours in a saturated solution of I_2 in methanol containing a trace of Br_2[7]. The central area of each view is shown at higher magnification in Figure 11. In each case, the upper picture shows the <111>A or growth surface, the lower picture shows the <111>B , the surface nearest the substrate. The stacking faults on the upper surface are longer than those on the lower, but the number density has decreased, indicating that many stacking faults are eliminated during the growth of the crystal.

The same views are shown again in Figure 12 after annealing 16 hours at 860° , 8 hours at 900° , repolishing and etching 15' in a warm $HF-HNO_3-AgNO_3$ solution. The apparent increase in dislocation etch pit density may be due to generation of additional dislocations but is more likely due to the better action of this etch in revealing them.

<u><111>B</u> . The stacking fault structure of the <111>B crystal (SC94-7<111>B , Tables II and IV), whose strain birefringence pattern is shown in Figure 7, is shown in Figure 13. The area shown is that under the triangular mesa shown (at half the magnification) in Figure 14. The stacking fault array is visible on the surface of the mesa. In the bottom view, Figure 13, taken with transmitted light the lines of emergence of the stacking faults on the opposite side are also faintly visible.

Several points should be noted. First the number density of stacking faults is far less than in the previous <111>A grown crystal. Again, a large number of the stacking faults initiated at the substrate interface are not propagated through the crystal. The development of a mesa seems to depend on some particular interaction of at least

two stacking fault arrays since many such arrays appear without associated mesas. The mechanism generating the mesa may under more severe conditions lead to a polycrystalline nodule.

Dislocation etching (under the same conditions described above for the <111>A crystal) reveals a very high dislocation density throughout the crystal except within the region of the mesa, as shown in Figures 15 and 16.

<u><100></u> . The strain birefringence patterns of Figure 8 were taken in the region of a stacking fault array at the center of a bump, one of the small dark spots in Figure 1. An enlarged view of one of these regions, showing clearly a number of lamellar twins in the array, is shown in Figure 17. The stacking fault and/or twinning patterns at each surface developed by etching in sodium hypochlorite solution are shown in Figure 18.

The pits produced on the upper <100> surface by etching in $HF-HNO_3-AgNO_3$, shown in Figure 19, resemble those described by Abrahams[8] using a somewhat different etch on GaAs <100> surfaces. Many run in the <110> direction and presumably, therefore, correspond to the usual 60° edge dislocations. Some polygonization is also evident.

<u><211>A</u> . The stacking fault and dislocation structure of a <211>A grown crystal (SC93-1<211>A, Tables II and IV) is shown in Figure 20. The treatment was the same as that described above for the <111>A crystal and the area shown is the same as in Figure 9. The etch did not develop dislocations clearly on the <211>B side of the crystal although the stacking faults are revealed. Almost all of the stacking faults are in the <111> plane perpendicular to surface and extend all the way through the crystal. As in the <111>A crystal with a high stacking fault density, the dislocation density is low.

Comparison of Figure 20 (top) with Figure 9 (bottom) shows

that most of the birefringence is associated with stacking faults in this <211>A crystal. The same is probably true of the <111>A crystal of Figure 6 although the one to one correspondence cannot be established. The high density of bright spots in the pattern of Figure 7 can be associated with nothing but the high density of dislocations revealed in Figures 15 and 16. The outline of the stacking fault array can be seen in the strain birefringence pattern of Figure 8, the central area being relatively free of strain. Strain patterns in other areas of the crystal are probably associated with dislocations.

While only a few selected samples have been examined, the main features are probably typical for crystals grown under similar conditions. (That changing the conditions can alter the structure is illustrated by the <111>A crystal, SC60-7, grown using PCl_3 under high temperature, fast growth rate conditions. Except in the vicinity of a step in the substrate used, this crystal had a very low dislocation and stacking fault density. See Figures 1 and 4, Ref. (2). The various structural features described, and others, undoubtedly play a part in the growth mechanism on different orientations and may play a part in the segregation of impurities responsible for the variation of electrical properties with orientation.

The effect of structure variations on solar cell characteristics has not been investigated directly because other factors appeared to be more critical. However, the presence of dislocations and stacking faults may be expected to have a strong influence on the formation and behavior of p-n junctions, and probably deserves more attention than it has been given.

G.   CLOSE-SPACE WATER VAPOR TRANSPORT

The close-space technique for epitaxial deposition[9] offers the advantages of simplicity and very efficient utilization of source material and so has been investigated as a method for growing single

crystal gallium phosphide. Details of the investigation are reported in Quarterly Report No. 1[2]. Thick layers, up to 0.4 mm, were made using either powder or polycrystalline ingot as the source. Major problems encountered were alloying, due to reaction with the substrate, poor structure, and inferior electrical properties and solar cell characteristics. Because of the limitation on purity imposed by the requirement of using a presynthesized source and the success in the open tube system in growing thick layers, the close-space work was discontinued.

IV.   SOLAR CELL FABRICATION AND EVALUATION

A.   INTRODUCTION

In the previous contract[1] GaP solar cells were developed which had conversion efficiencies under usual sunlight intensities (75-90 mw/cm^2) of about 1% and open circuit voltages up to 1.35 volts with a short circuit current density of 1.4 ma/cm^2. At 350° C, a V_{oc} of 0.4 volts was obtained. In the course of work on this contract, the conversion efficiency has been increased to 1.9%, the V_{oc} to 1.40 volts, the J_{sc} to 1.6 ma/cm^2 and at 350° C, a V_{oc} of 0.45 volts has been obtained.* These advances have resulted largely from improvement in the material purity and development of better solar cell fabrication techniques.

This portion of the report will summarize the solar cell fabrication and evaluation of GaP solar cells and emphasize some of the problems connected with the development of efficient high temperature cells.

The study of the fabrication procedure has involved an optimization of the diffusion schedule and improvement of the top contact to the p layer. In addition, work has been conducted with diffusants other than zinc. Annealing experiments have also been carrier out.

The optimization of the diffusion parameters was undertaken in the hope of reducing or eliminating the high internal series resistance found in the GaP junction and believed to be at the core of the problem that has to be resolved before highly efficient GaP cells can

---

*   * From solar cell theory, the following solar cell characteristics for GaP would be anticipated at room temperature:

$$V_{oc} = 1.7 \text{ volts}$$
$$J_{sc} \cong 8 \text{ ma/cm}^2$$
$$n \cong 8\%$$

be developed[2]. Series of experiments detailed in the first quarterly report[2] indicated that indeed the internal series resistance could be reduced somewhat but not eliminated by altering diffusion conditions. It was found that a shallow diffusion at 800° C for 3 minutes with a p /Zn atomic ratio of 0.66 led to the lowest junction series resistance and to the best solar cells. This result was adopted as standard procedure in our cell fabrication[1]. A further improvement was effected by adopting a nickel-silver contact to the p layer in place of previously used silver.

In an effort to overcome the series resistance in the junction, different p type diffusants have been tried, namely, cadmium and magnesium. Neither has produced any improved solar cell results. The work on cadmium has been reported in the previous final report[1], page 69. The magnesium diffusions are reported in Table VII. Attempts have also unsuccessfully been made to alloy with tin into p-type GaP[2]. In every case the junctions produced thus far by these other dopants have been inferior to those made using the optimized zinc schedule.

Another method of forming junctions in GaP presently being investigated is that of ion implantation[4]. As yet no results have been obtained on samples of GaP sent out for ion implantation studies.

At present, a technique for controlling, fabricating and reproducing good p-n junctions suitable for high efficiency GaP solar cells from material presently available has not been developed. The best junctions have been characterized in terms of p-i-n structures with the i layer width(d) considerably larger than the diffusion length (L_i)[3]. Carrier lifetimes $\leq 10^{-9}$ sec have been deduced by various methods. (See Ref. 2, p. 29 and Ref. 3, p. 27) Capacity-voltage data has also substantiated the effect of wide i layers, and a $\frac{1}{c^3}$ dependence is quite common. Current-voltage characteristics have indicated for the best cells an n = 2 in the expression $J = J_o \exp \frac{ev}{nkt}$ where J is the current density, J_o is the saturation current density,

V is the applied voltage, and T is the absolute temperature, while the value of n = 2 is an indication of a non-ideal junction, it is also to be pointed out that the areas under investigation have usually been of the order of .1 cm^2 , a considerably larger area than normally worked on for many other applications (Ref. 2, p. 50; Ref. 3, p. 46).

The implied connection between the i layer and the series resistance in the junction has led to the thought that the i layer width (or series resistance) can be reduced or suitably minimized by utilizing a high level of carrier generation, i.e., a high intensity source. An increase in conversion efficiency may be expected under such conditions. Solar cells have been subjected to sunlight intensities as high as 500 mw/cm^2 and tungsten intensities higher than 100 mw/cm^2 (Ref. 2, Fig. 9). In Figure 21, a plot is shown of the conversion efficiency for various GaP solar cells as a function of solar intensity. (The measurements were made in sunlight with the aid of a parabolic mirror.) The intensity was calibrated using a standard silicon solar cell of 10% efficiency and making use of the linear relationship between short circuit current density and intensity. Several of the GaP solar cells show increasing efficiency with increased solar intensity. For Sample NA68 SC76-4 an efficiency of better than 3.5% is indicated at an intensity of 200 mw/cm^2 with a decrease on application of higher intensities. On the other hand cell NA76 SC93-6 shows a continual decrease in efficiency with increasing intensity. Most of the cells show an increase as the intensity is increased at least to a certain level. Sample NA75 SC91-6 is a GaAs$_{.43}$P$_{.57}$ alloy which has been included. It is noted that an efficieny over 5% is observed for this cell at about 400 mw/cm^2. Further remarks on GaAsP alloy cells will be made in a later section.

Another method for reducing or altering the i layer or series resistance that has been attempted is the use of heat treatment. Annealing experiments at 850° C (with rapid cooling)[3] proved to be

unrewarding as the solar cell and junction characteristics showed. It is obvious that the proper conditions were not obtained.

The nature and possible cause of the i layer (or series resistance) was investigated[3] using the optical absorption coefficient as a tool. Two sets of experiments were conducted. In the first experiment, the absorption coefficient of a number of (1) epitaxial GaP samples prepared by different methods and (2) of GaP prepared by crystallization of GaP from the melt were investigated over a range of wavelengths from $0.50\,\mu$ to $12\,\mu$. These measurements indicated that there were large differences in the absorption coefficient depending on the methods of crystal preparation. It was also noted from the analysis of the absorption coefficient (at a single wavelength--$0.6\,\mu$ was used) vs. carrier concentration, there appeared to be, in the starting material, a background level of $\leq 10^{15}$ carriers/cm^3 present in all the material which was believed due to deep level impurities, vacancies and/or compensation effects. (Work to be described later pointed to oxygen, a deep level impurity as being one of the impurities present in our material.)

The second experiment (Ref. 3, pp. 20-24) utilized the effect of diffusing zinc into the starting GaP by simulating the diffusion schedule (800° C for 3 minutes). The optical absorption coefficient (between 0.50 and $0.65\,\mu$) was measured (1), initially (2), then with zinc diffused in and (3) after removal of zinc. The measurements were displayed in Figures 17 through 23 of the second quarterly report[3] for a number of GaP samples and showed, in some cases, surprisingly large final changes from the initial value, either as an increase or decrease, in the absorption coefficient. These changes were interpreted as being due largely to the background level ($\leq 10^{15}$/cm^3) of the starting GaP (presence of deep level impurities and compensating impurities). It was suggested that because of the small values of the intrinsic concentrations of charge carriers in these materials, they are not yet intrinsic at the temperatures at which it is technologically possible to prepare p-n

junctions. Therefore these junctions have a built-in electric field at the temperature at which they are prepared which is in general high enough to render part of the impurities mobile. Consequently, during the process of fabrication, an ion drift type* of phenomenon may occur which could lead to p-i-n type of structures.

A reasonable correlation of the change in optical absorption coefficient (expressed in terms of a ratio) and the short circuit current density of the solar cell was seen (Ref. 3, Table VIII). As previously noted, (Ref. 3, p. 25) an increase in solar cell short circuit current density is associated with a decrease in i layer width (or series resistance). The change in absorption coefficient ratio is then related to the i layer width and effect of "mobile" impurities on the formation of this i layer.

Clearly, the width of the intrinsic or i region depends strongly on the temperature at which the crystals are prepared and on their subsequent thermal history. If the junctions could be prepared at temperatures at which the material is intrinsic, quenching could perhaps be used to prevent the formation of an intrinsic region. Since GaP becomes intrinsic at or near the melting point, practical difficulties make this approach unappealing for solar cell work. Use of heavy doping which reduces the width of the i layer, has limitations for solar cell use inasmuch as carrier absorption becomes excessive and the lifetime being a function of concentration tends to decrease with high concentration adversely affecting the short circuit current[3].

The set of experiments recounted provide evidence that the solar cell characteristics have been controlled and limited by an i layer (or series resistance) which has its origin in the bulk material and appears as part of a background level of $\leq 10^{15}$ carriers/cm^3 in the

---

* Precipitation effects and stress fields in the crystal are also intended to be included in the general realm of ion drift effects.

initial bulk material. Fabrication of a p-n junction using zinc diffusion techniques tends to emphasize the i layer (and series resistance) since mobile impurity ions and compensation effects are quite likely at the normal diffusion temperature used. At higher diffusion temperatures, shallow junction depths become more difficult to control.

B.   MEASUREMENT OF ELECTRICAL PROPERTIES OF GaP AND AN ASSESMENT OF IMPURITIES

Of the two approaches followed in this study, only the first approach which emphasized junction fabrication procedures and problems has been discussed. The second approach, dictated by the above experiments relating to an inherent background level in the starting material, was undertaken to characterize and study the impurities in the bulk material and to assess the guide used for judging purity in the GaP, namely, the room temperature mobility.

Hall effect and resistivity were measured as a function of temperature, from liquid nitrogen to 120° C, on three GaP samples, chosen because they gave rise to the best solar cells. These samples, all single crystals, were SC76-4<111>B, SC77-4<111>B and SC90-6<111>B. Solar cells made from these materials gave rise to conversion efficiencies (in sunlight) between 1.2 and 1.9% (see Table VIII). In addition to Hall effect and resistivity and solar cell characteristics, spectroscopic emission analysis and electroluminescence data   accumulated and efforts made to correlate the findings.

Samples of dimensions of the order of .8 x .3 x .035 cm^3 were used for Hall effect and electrical resistivity measurements. Electrical contacts were made to the GaP samples with indium which was evaporated and alloyed into the sample at about 500° C. All of the samples measured displayed n type conductivity.

The curves of Hall constant and electrical resistivity as a function of temperature obtained on the three GaP samples are displayed

in Figures 22, 23 and 24 respectively. It is noted that in each case the shape of the resistivity and Hall effect follow each other fairly closely. The resistivity reaches a minimum at about 200° K for each of the three samples and then starts to increase with increasing temperature. The Hall coefficient decreases more slowly at temperatures above 250° K and appears to show a tendency to flatten out (exhaustion range) somewhat above room temperature. The Hall constant of Sample SC90-6 <111>B shows two slopes, one being about half the other. The first slope has an activation energy of .057 e.v. From a replot of the Hall curve as $nT^{-3/2}$ vs. $1000/T$, we note the second slope is 0.11 e.v. which within experimental error is about double the first slope*. One can, as will be shown later, interpret these energies with the aid of the dissociation equation[10], the relative concentrations of n, the electronic carrier concentration in the conduction band, N_A, the acceptor concentration and N_D, the donor concentration. In addition, using the assumption that the density of states effective mass, $m^* = m_o$, the free electron mass, nondegeneracy and the assumption that $n = \dfrac{1}{Re}$, it follows that the smaller slope is half the ionization energy of the impurity and that the larger activation energy 0.11 e.v., indicates the donor impurity ionization energy.

Samples SC77-4<111>B and SC76-4<111>B, Figures 23 and 24, show only one activation energy on the $\ln R$ vs. $1000/T$ curves. The donor activation energy is the same for both samples, namely .08 e.v. Donor ionization energies of .11 e.v. and .08 e.v. are noted for these three samples. SC90-6 was prepared using trichloro-ethylene transport whereas SC76-4 and SC77-4 were grown using $AsCl_3$ as the transport agent.

In attempting to correlate the donor impurities corresponding to these energies with that found from emission analysis (Tables VIII,

---

* The appearance of a hump between the two slopes in Figure 22 has not been explained.

IX, X), it is of interest to first deduce the donor and acceptor concentrations from electrical data and then compare with emission analysis.

The concentration of p-type and n-type impurities contained in a sample can be computed from Hall data. This method makes use of the dissociation equation[11]. N_A and N_D are then calculated from the temperature dependence of the concentration of charge carriers, from the extrapolated value of the $\ln nT^{-3/2}$ vs. $1/T$ curve at $1/T = 0$, and from a knowledge of the exhaustion range. It is also assumed that the density of states effective mass, m^*, is the same as the free mass, m_o.

The values of N_D, N_A for the three Samples SC90-6, SC77-4 and SC76-4 deduced from the Hall data are shown in Table VIII. In the case of SC90-6, use was made only of the dissociation equation and the two cases applying to the two slopes i.e., $n \gg N_A$ and $n \ll N_A$. For Samples SC76-4 and SC77-4 use was made of the condition $n \ll N_A$ and the condition at the exhaustion region $(n_{ex} = N_D - N_A)$. For Sample SC90-6, a donor concentration of $N_D = 1.2 \times 10^{17}/cm^3$ was deduced which cannot be correlated with the impurity levels found from emission analysis and presented in Table VIII for this sample. However, from the literature it would appear that the activation energy of 0.11 e.v. found for this donor level is close to that reported for sulfur[11]. Since sulfur is not detected readily by emission and the other impurities are, acccording to the emission analysis, present at low levels, it is likely that the major donor impurity present in SC90-6 is sulfur. The acceptor value of $8.4 \times 10^{14}/cm^3$ deduced from the Hall data is very low, over an order of magnitude below that noted from emission for the likely acceptor candidate--magnesium. This puzzling point will be discussed below.

Surprisingly good agreement is noted between emission analysis and Hall data for Samples SC77-4 and SC76-4. These results indicate silicon to be the dominant donor impurity and the activation

energy of .08 e. v. would be assigned to silicon. This conclusion is in reasonable agreement with the work of Gershenzon, et. al.[11].

Hence, shallow donor impurities present in the GaP samples are sulfur and silicon.

Of the possible shallow acceptor impurities in these samples, as noted from emission analysis, magnesium and calcium (with concentrations above the confidence level of the analysis) are logical condidates. However, the concentrations of these impurities when compared with N_A , deduced from Hall data, do not provide a good correlation, especially for Samples SC90-6 and SC77-4. An interesting possibility to correlate the data of Table VIII is that silicon might be present as an acceptor in addition to its donor capability[11]. If the ratio of Si atoms/cm^3 of SC76-4 and SC77-4 found from emission analysis is compared with the ratio of the acceptor concentration of SC76-4 and SC77-4 deduced from Hall data it is noted that they are the same. Further the ratio of green/red electroluminescence (see Table VIII) for these samples i. e., $\frac{SC76-4}{SC77-4}$ decreases in about the same ratio as the presumed silicon acceptor concentration increases. In the case of Sample SC90-6, the concentration of the donor impurity, sulfur, is so much larger that the effect of silicon may not readily be noted although the small acceptor concentration might suggest that the ratio of $\frac{Si\ donor}{Si\ acceptor}$ decreases with increasing silicon concentration as one proceeds from Samples SC90-6 to SC76-4. Some of the magnesium might also be electrically active since it is reported to be an acceptor[11]. However, there is difficulty in explaining the calcium and its role electrically. It is of interest to mention that the calcium content was found to decrease drastically for epitaxial GaP prepared using water vapor transport[4].

Shallow acceptors in these GaP samples appear to be silicon and likely magnesium.

The roles of the other impurities noted from the emission

analysis of Table VIII such as Al, Ag are not clear. The role of Cu is believed to be as a deep level[13] although its exact role has not been elucidated.

The presence of oxygen, a deep level impurity and its effects on the solar cell characteristics are reviewed further below.

From Table VIII, a correlation will be noted between the total ionized impurity content (N_I) and the conversion efficiency (in sunlight, normal intensities of $\sim 80\text{-}90$ mw/cm^2). The sample with the lowest N_I has the highest conversion efficiency (SC77-4). The oxygen content is also less than for the other two samples as judged from the electroluminescence green/red ratio > 1 *.

An impurity, which has been shown by Gershenzon, et. al.[11, 12] to be present in GaP as a deep level is oxygen. This was investigated in the grown material for its possible effect on the solar cell charact-eristics. As reported in the third quarterly report[4], using electro-luminescence to detect the presence of oxygen, it was noted that the open circuit voltage of cells prepared from epitaxial GaP grown using water vapor was significantly lower than GaP made epitaxially but using a chloride transport. From electroluminescence data, it was deduced that the GaP prepared via water vapor transport had a signifi-cantly higher oxygen content than GaP prepared by chloride transport. The experiment provided support for the presence of the deep level impurity oxygen. Its exact role in the i layer (or as a contributor to the series resistance) of the junction has not been established, especially as the short circuit current denisty did not show any orderly variation with oxygen content[4]. Some of the reason may lie in the role played by the shallow levels, i.e., both donors and acceptors present in all the epitaxial material. Further, the electrical role of oxygen in GaP is not clearly established especially as it relates to the

---

* Sample SC90-6 has been only qualitatively examined, but it is noted that the green/red ratio < 1.

possibility of oxygen occupying both substitutional and interstitial sites and having multiple ionization levels.

Other deep level impurities and aggregates as well as vacancies and other imperfections which may give rise to deep level effects have yet to be investigated and correlated with p-n junction and solar cell characteristics.

A second procedure for determining the concentration of ionized impurities, N_I, is to make use of the mobility. From the Brooks-Herring relation[14], one can determine a value of N_I. The Hall mobilities, R/ρ, for the three samples, SC90-6, SC77-4 and SC76-4, are plotted as a function of temperature in Figure 25. The curves follow a $T^{-1.9}$ law from about 120° K to the highest temperature measured ($\sim 400°$ K).

From the measured Hall mobility and assuming that the mobility contributions can be accounted for by lattice (optical mode) scattering and impurity scattering and using the F relationship compiled by Johnson and Lark-Horovitz[15], as well as taking the conductivity effective mass, $m^* = .35 m_o$ (for electrons), one can compute values of N_I for the various Hall mobilities at the various temperatures. This is reported below for the three samples SC90-6, SC77-4 and SC76-4 at 300° K and compared with N_I deduced from Hall data and with the impurities deduced from emission analysis.

Comparison of N_I Deduced by Different Methods

for Samples SC90-6, SC77-4, SC76-4

	N_I(Mobility), no/cm³	N_I(Hall), no/cm³	N_I(Si Anal.), no/cm³
SC90-6<111>B	6.6×10^{16}	6.0×10^{16}	$\sim 9 \times 10^{15}$
SC76-4<111>B	1.89×10^{17}	6.8×10^{16}	1.25×10^{17}
SC77-4<111>B	2.5×10^{16}	3.1×10^{16}	4.5×10^{16}

While the agreement appears to be reasonably good, it is thought to be fortuitous. A consistent fit, using optical and impurity scattering only, has not been obtained with the experimental mobility over the range of temperatures. It is felt that the mobility analysis is incomplete and requires further study.

The blind use of the Hall mobility as a guide to purity at room temperature may be misleading since optical mode scattering dominates (except for extremely high impurity content) and with the electron effective mass, m^* taken to be equal to $.35 m_o$, a value for the electron lattice mobility μ_o (optical mode or polar scattering mobility) of 174 cm^2/volt sec at 300° K is calculated. Some of the samples noted in our previous reports have approached this value. To use the Hall mobility as a sensitive guide of impurity content a measurement at a temperature where impurities dominate, i. e., below room temperature, might be a better indication. For examples, from Figure 25 we note that at 77° K SC77-4 has the highest mobility, $\mu = 1450$ cm^2/volt sec, while Samples SC90-6 and SC76-4 have mobilities (at 77° K) of 1300 and 730 cm^2/volt sec respectively. The decrease in mobility noted agrees with the increase in N_I found in the table above using Hall and mobility data at 300° K.

C. GaP SOLAR CELL EVALUATION: ROOM TEMPERATURE AND ABOVE

Solar cells made from epitaxial GaP prepared using $AsCl_3$ transport gas have given the best solar cell characteristics obtained. These data are reproduced below including the spectral response, high temperature properties and cell area (also see the third quarterly report[4] and parts of Table VIII, this report).

	Sample	
	NA68 SC76-4	NA68 SC77-4
V_{oc}* (volts)	1.40	1.38
J_{sc}* (ma/cm^2)	1.43	1.60
Spectral Response Peak (microns)	.45	.45
Cell Area (cm^2)	.45	.37
β, Temp. Coefficient V_{oc} (mv/deg)	3.0	3.3
$V_{oc}\pm$ at 350° C (volts)	.45	.42
$J_{sc}\pm$ at 350° C (ma/cm^2)	1.36	1.51
Conversion* Efficiency (%)	1.5	1.9

* measured in sunlight, solar intensity as measured with silicon solar cell was 83 mw/cm^2.

± measured with tungsten source.

The epitaxial GaP was doped with silicon in these samples as noted in the previous section. The total ionized doping concentration in SC77-4 is the lowest thus far obtained and could account for the higher efficiency observed.

GaP samples prepared using chloride transport have generally given better solar cell characteristics (V_{oc}, J_{sc}) than those using water vapor as the transport agent. This is especially true at the higher temperatures[4].

While the hoped-for 0.7 volts (for V_{oc}) at 350° C has not been achieved, generally improved high temperature properties have been noted as the material quality has been improved[4]. Using the chloride process and especially $AsCl_3$ as the transport agent (in preparation of GaP), the J_{sc} of solar cells fabricated from this material show a continuous increase* to 350° C as opposed to the more usual saturation at a lower temperature (~250° C) and a rapid decrease thereafter.

At the present stage of development of fabrication procedures and material development, an upper temperature limit for GaP solar

* measured using tungsten source.

cells of 350° C has been noted[2]. At present, zinc migration (see following section) and the problem of suitable high temperature contacts limit the temperature of operation to 350° C. As both fabrication procedures and material development improve, this limitation should be raised.

A list of GaP solar cells fabricated and evaluated during this last quarter are given in Table IX. Previous cell fabrications and evaluations are found in the proceeding three quarterly reports.

D. ADDITIONAL FACTORS CONTROLLING GaP SOLAR CELL CHARACTERISTICS

During the course of this work, possible deleterious effects of structure defects and material inhomogeneity on the solar cell characteristics have been pointed out. Work on structural defects in GaP has also been presented in an earlier section of this report.

One of the manifestations of material inhomogeneity (and non-equilibration) has been an irreversibility noted in the GaP solar cell characteristics on continued heating and cooling of the solar cell[2].

Irreversible changes in carrier concentration on heat treatment of bulk GaP has also been observed[3].

At temperatures above 400° C, solar cell deterioration is believed mainly attributable to zinc migration[2]. The tendency of zinc to collect at defects and dislocations which arise from structure deficiency on material inhomogeneity could be the source of the zinc atoms which migrate. The limitation of the present GaP solar cells employing zinc to temperatures of 350° C as previously mentioned is a result of this effect.

E. GaAs-P SOLAR CELL EVALUATION

Some evaluation work has been carried out on single crystal $GaAs_{(1-x)}P_x$ solar cells ranging in concentration from x = .12 to

to x = .84 . The fabrication procedure was previously described[4].
Essentially, p-n junctions have been made by diffusing zinc from a
$ZnAs_2$ source at 875° C for 3 minutes into the alloy.

The spectral response peak of the cells shifts to shorter wave-
lengths with increasing phosphorus content as expected. Best efficiency
performance has been obtained with composition $GaAs_{.43}P_{.57}$. (Sample
NA75 SC91-6, see Table X) A conversion efficiency of 1.3% was noted
in sunlight for a solar intensity of 80 mw/cm² (as measured with a
standard silicon cell). On application of higher intensity (see Figure
21) the efficiency was noted to rise to about 5% at 400 mw/cm² , which
demonstrates that promising characteristics can be achieved with GaAs-P
solar cells. Obviously, the characteristics of the cells summarized in
Table X are dependent upon some uncontrolled factors in the material.
The only characteristic that appears to be dependent on composition is
the spectral response peak. Improvements in the quality of the GaAs-P
material need to be achieved before the full potential of GaAs-P for solar
cell application can be assessed.

At higher temperatures, the properties of GaAs-P have been
found to be inferior to thos of GaP.

A list of the GaAs-P samples evaluated on the contract is
shown in Table X.

V.   CONCLUSIONS

A.   MATERIAL PREPARATION

The highest purity and best solar cell performance have been obtained in <111>B crystals grown at low temperature and low growth rate in quartz, using high purity arsenic chloride as the transport agent source. High purity chlorinated hydrocarbons such as trichloroethylene may serve equally well as the source of transport agent, although carbon contamination from these sources might ultimately be found to introduce a limitation on solar cell performance.

The PCl_3 used in this work apparently introduced some contamination into the GaP which adversely affected solar cell performance, but ultimately high purity PCl_3 should provide the most convenient source of both transport agent and phosphorus. Although relatively good solar cell performance was achieved by tellurium doping of water vapor transported GaP, the oxygen contamination did appear to adversely affect open circuit voltage.

Emission spectroscopic analyses have shown the purity of the vapor grown GaP crystals to be orders of magnitude higher than previously assumed so that the problem of further increasing the purity is greatly magnified. Use of a BN tube liner, rather than improving the purity, introduced some unidentified contaminant which adversely affected the solar cell characteristics.

The pronounced effect of growth orientation on electrical properties has been confirmed and correlated with its effect on the segregation of silicon in undoped crystals and of tin in heavily tin doped crystals.

The effect of the transport system used on the structure of crystals of various orientations is a manifestation of differences in impurity content of the gas streams.

Strain, associated with stacking faults and dislocations, has been found in crystals of several orientations. Very high dislocation

densities, as found in a <111>B crystal, may have an effect on the forma-
tion and behavior of p-n junctions. High stacking fault densities, as found
in <111>A and <211>A grown crystals, may have contributed to poor solar
cell performance from these orientations.

Perfection of the close-space water vapor transport system
presents formidable problems of control and purity--limited by the
requirement of a presynthesized source. This system, therefore, is not
as attractive as the open tube system.

B.   SOLAR CELL FABRICATION

Improved GaP solar cells have been developed, the best having
had room temperature conversion efficiencies in sunlight (80-90 mw/cm^2)
of almost 2%. Open circuit voltages and short circuit current densities,
especially the latter at the higher temperatures, have increased. These
improved characteristics have resulted from obtaining purer material,
and improving the solar cell fabrication technique by optimizing the
diffusion schedule and forming more stable contacts to the p layer.

The best cells have been obtained from material having a total
ionized impurity concentration, N_I, of 3 x 10^{16}/cm^3 which is consider-
ably lower than previously obtained. Silicon was the dominant impurity
and the oxygen content, as deduced from electroluminescence, was
among the lowest of any of the samples from which solar cells have been
made and analyzed.

There is evidence that GaP solar cell conversion efficiencies
increase to better than 3.5% under the influence of higher solar
intensities. This suggests that with further improvement in fabrication
techniques and material control and purity, considerable improvement
in the conversion efficiency and solar cell properties can be expected
at solar intensities (80-90 mw/cm^2) normally used for testing.

Aside from the problems connected with growing of GaP
single crystals there are two areas where additional effort could result.

in further improvement in GaP solar cells.

A thorough examination should be made of the electrical and optical properties of single crystal GaP so that the material can be adequately characterized, and suitable evaluation guides established which would aid in finding the best fabrication techniques for making solar cells. A start has been made in this direction under this contract. The roles of some of the impurities such as Si , S and oxygen on the solar cell properties have been intimated. The use of the Hall mobility at low temperatures as a guide to material purity has been suggested. In addition, the role of vacancies has been intimated in an earlier report. Much more detailed work remains to be done and a great number of confirmatory and correlatory experiments especially with the fabricated solar cell have to be carried out to aid in selecting and controlling the material.

An improved method for fabricating large area junctions in this high bandgap semiconductor, by which p-n rather than p-i-n structures can be fabricated, at temperatures below which the material becomes intrinsic, but at which it is technologically possible to prepare junctions, needs to be developed.

VI.   RECOMMENDATIONS

Epitaxial deposition on GaAs substrates via the open tube chloride transport system offers the best route to high quality large area single crystal GaP. Additional work needs to be done to define the optimum conditions for growth. This may include detailed kinetic and thermodynamic studies of the transport reactions and investigation of the mechanism of crystal growth.

The apparatus should be redesigned to permit better control of temperatures and temperature gradients, of flow rates and flow patterns. This is necessary to achieve control of and uniformity of properties of large area crystals. Provision for chemical vapor etching of substrates immediately prior to deposition should be included.

Efforts to improve purity should include purification of PCl_3 for use as the transport agent and phosphorus source. Alternatively, high purity HCl gas might be generated and employed with purified phosphine.

Silicon contamination from reactions with quartz does not appear to be a serious source of contamination at the relatively low temperatures employed in the vapor transport system so quartz can be used as a material of construction.

A detailed study of the structural, electrical and optical properties of single crystal GaP so that the nature and role of some of the impurities and defects can be identified and assessed is important if further progress is to be made in the technology of the material. Correlation of these properties with emission data, electroluminescence characteristics, solar cell characteristics , and other junction properties would provide a good start on the control of the material and on the proper fabrication procedures to use for the application of GaP to devices such as solar cells.

Improved methods of making junctions in GaP which would minimize the effect of the i layer would lead to improved solar cell efficiencies.

VII.   SAMPLES SUBMITTED TO NASA

During the contract period 24 samples were submitted to Lewis Research Center, NASA, as follows: 4 GaP single crystals, 4 GaP single crystals with diffused p-n junctions, and 16 solar cells complete with electrical contacts and collector grids. The characteristics are listed in Table XI.

VIII.   REFERENCES

1.   "Development of Improved Single Crystal Gallium Phosphide Solar Cells" Final Report, June 12, 1963 - August 12, 1964, Contract No. NAS3-2776, NASA CR-54273.

2.   Quarterly Report No. 1, 15 August - 15 November, 1964, Contract No. NAS3-6014, NASA CR-54241

3.   Quarterly Report No. 2, 15 November - 15 February, 1965, Contract No. NAS3-6014, NASA CR-54338.

4.   Quarterly Report No. 3, 15 February - 15 May, 1965, Contract No. NAS3-6014, NASA CR-54427.

5.   C. D. Thurmond and C. J. Frosch, J. Electrochem. Soc. $\underline{111}$, 184 (1964).

6.   Data Sheet, BORALLOY Boron Nitride, High Temperature Materials, Inc. February 1, 1965.

7.   M. Gershenzon and R. M. Mikulyak, J. Appl. Phys. $\underline{35}$, 2132 (1964).

8.   M. S. Abrahams I-E, Technical Report No. 2, December 15, 1964, Contract No. SD-182, ARPA Order 446, Radio Corporation of America.

9.   F. H. Nicoll, J. Electrochem. Soc. $\underline{110}$, 1165 (1963).

10.   Semiconductors, edited by N. B. Hannay, p. 30, Reinhold Publishing Corporation, New York (1959).

11.   M. Gershenzon and R. M. Mikulyak, J. Appl. Phys. $\underline{32}$, 1338 (1961); Solid State Electronics $\underline{5}$, 313 (1962).

12.   M. Gershenzon, R. M. Mikulyak, R. A. Logan and P. W. Foy, Solid State Electronics $\underline{1}$, 113 (1964).

13.   J. W. Allen and R. J. Cherry, SERL Tech. J. $\underline{13}$, 57 (1962); Cherry, R. J. and J. W. Allen, Int. Conference on the Physics of Semiconductors, Proc. Held at Exeter, July, 1962. Ed. by Stickland, A. C., London, Inst. of Phys. and the Phys. Soc., 1962, p. 752-759.

14.   F. Blatt, Advances in Solid State Physics, Vol. 4, p. 200-366, Ed. by F. Seitz and D. Turnbull, New York (1957).

15.   V. A. Johnson and K. Lark-Horovitz, Phys. Rev. $\underline{82}$, 977 (1951).

14.   F. Blatt, Advances in Solid State Physics, Vol. 4, p. 200-366, Ed. by F. Seitz and D. Turnbull, New York (1957).

LIST OF TABLES

TABLE I

Systems Employed for Vapor Transport and Epitaxial Growth of Single Crystal GaP

Transport Agent Source	No. of Runs	Phosphorus Source	No. of Runs	Gallium Source

```
PCl3 ————————(10)————————> PCl3
C2HCl3 ———————(8)————————> P(Red)         (10)
                  (10)                      (24)
AsCl3 ————————(2)————————> PH3 ————————(2)————————> Ga
                  (6)
                  (2)                  P3N5          (1)
                  (1)
H2O ————————(2)————————> GaP ————————(4)————————> GaP
```
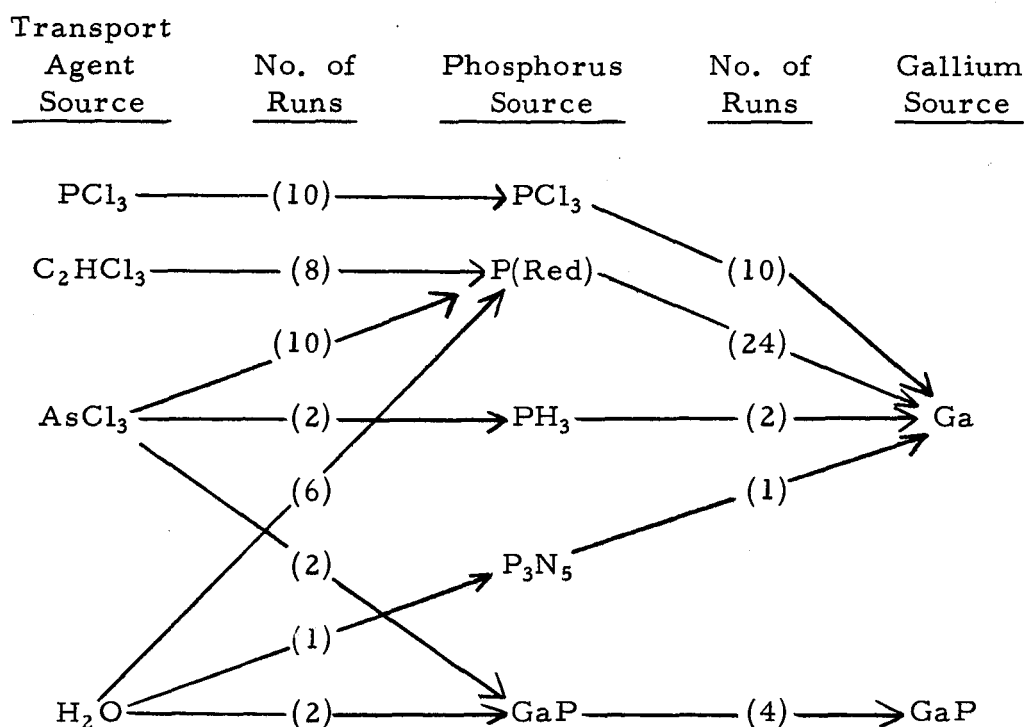
PCl3 :   Mallinckrodt, Analytical Reagent Grade.

Trichloroethylene: Mallinckrodt, TransistAR Grade.

AsCl3 :   Cominco Products Inc., High Purity.

H2O :   distilled and deionized.

P(Red) :   American Agricultural Chemical Company, semiconductor grade.

PH3 :   Matheson, semiconductor doping gas, 1% mixture in ultrapure hydorgen.

P3N5 :   Cerac, Inc., semiconductor doping grade "spectroscopically pure".

TABLE I
(continued)

GaP :   Monsanto Co. polycrystalline ingot.

Ga :   Alcoa, 99.9999%; AIAG, high purity,
semiconductor grade, 99.9999%.

TABLE II

Vapor Transport of GaP Using HCl[1]

Run No.	Source Temp (°C)	Low Substrate Temp (°C)	H_2 Flow Rate (cc/min)	Pressures (atm x 10^3)			Time (min)	Source Loss (gm)	Substrate Gain (gm)	% Yield
				Initial HCl	Initial P_2	$GaCl_x$ at Source				
AP138	894	771	280	4.2[2]	2.0	3.4	5990	17.27	6.83[3]	27.4
SC91	890	798	270	2.7	0.44[4]	2.4	5554	11.25	1.46[5]	7.6
SC92	893	785	190	6.3	3.8	3.5	5961	12.06	3.08[6]	17.7
SC93	901	770	280	5.5	2.0[7]	4.1	4093	14.47	5.22[3]	25.0
SC94	901	758	280	5.9	2.4	4.1	4170	14.82	5.99[8]	28.0
AP139[9]	899	743	290	5.6	1.9[7]	4.0	4428	15.77	6.34[3]	27.8

(1) HCl from H_2 reduction of $AsCl_3$, except in AP138 in which trichloroethylene was the source.

(2) Trichloroethylene partially cracked @ ~1000°, passed through dry ice cooled trap.

(3) Substrates supported vertically, parallel to gas flow, BN support.

(4) Alloy run, 0.45×10^{-3} atm equivalent of As_2 from $AsCl_3$. $P/(P + As) = 0.495$

(5) Substrates supported horizontally, BN support. Alloy composition, 60.5 mole % GaP on <100>, 56.5% on <111>B.

(6) Substrates supported at 30° angle to flow, BN support, <111>B only surfaces exposed.

(7) P_2 from decomposition of PH_3, introduced as 1% mixture in H_2.

(8) Substrates supported vertically, parallel to gas flow, BN support. <111> wafers back to back to expose <111>B surfaces only.

(9) Sn doping, Sn source at 350° C in gas stream. Equivalent doping concentration, 1×10^{20} atoms/cm³ GaP.

TABLE III

Typical Electrical Properties of Undoped

Vapor Grown Epitaxial GaP Crystals

Substrate Orientation	System	Resistivity (Ω cm)	Mobility (cm^2/volt-sec)	n, Net Carrier Concentration (cm^{-3})
<100>	HCl , P , Ga	3	100	2×10^{16}
	PCl$_3$, Ga , low temp.	hi ρ - 8	hi ρ - 150	$<5 \times 10^{15}$
	PCl$_3$, Ga , high temp.	1.4	75	6×10^{16}
	C$_2$HCl$_3$, P , Ga, low temp.	hi ρ - 4500	hi ρ - 24	6×10^{13}
	C$_2$HCl$_3$, P , Ga , high temp.	3	200	1×10^{16} p
	AsCl$_3$, P , Ga	hi ρ - 130	hi ρ - 100	$<5 \times 10^{14}$
	AsCl$_3$, PH$_3$, Ga	hi ρ	---	---
	H$_2$O , P , Ga	hi ρ	---	---
	H$_2$O , GaP	hi ρ	---	---
<111>B	HCl , P , Ga	0.004	90	1.6×10^{18}
	PCl$_3$, Ga , low temp.	$2 \times 10^{\pm 1}$	160	$2 \times 10^{16 \pm 1}$
	PCl$_3$, Ga , high temp	0.12	120	4×10^{17}
	C$_2$HCl$_3$, P , Ga , low temp.	0.7	125	7×10^{16}
	C$_2$HCl$_3$, P , Ga , high temp.	1.0	150	4×10^{16}
	AsCl$_3$, P , Ga	0.8	150	5×10^{16}
	AsCl$_3$, P , Ga , BN tube	2	125	2.5×10^{16}
	AsCl$_3$, PH$_3$, Ga	4	165	1.5×10^{16}
	H$_2$O , P , Ga	hi ρ	---	---
	H$_2$O , GaP	hi ρ	---	---
<111>A	HCl , P , Ga	3000	10	2×10^{14}
	PCl$_3$, Ga , low temp.	hi ρ	---	---
	PCl$_3$, Ga , high temp.	85	120	6×10^{14}
	C$_2$HCl$_3$, P , Ga , low temp.	hi ρ	---	---
	AsCl$_3$, PH$_3$, Ga	hi ρ	---	---

TABLE III

(continued)

Typical Electrical Properties of Undoped

Vapor Grown Epitaxial GaP Crystals

Substrate Orientation	System	Resistivity (Ω cm)	Mobility (cm²/volt-sec)	n, Net Carrier Concentration (cm⁻³)
<111>A (continued)	H_2O , P , Ga	hi ρ	--	--
	H_2O , P , Ga	hi ρ	--	--
<110>	HCl , P , Ga	0.3	60	3×10^{17}
	PCl_3 , Ga , high temp.	1.4	60	5×10^{16}
	H_2O , GaP	hi ρ	--	--
<211>B	C_2HCl_3 , P , Ga , low temp.	10	160-70	$4\text{-}9 \times 10^{15}$
	C_2HCl_3 , P , Ga , high temp.	77±	60±	$1 \times 10^{15}±$
	$AsCl_3$, PH_3 , Ga	14	86	5×10^{15}
	H_2O , GaP	hi ρ	--	--
<211>A	C_2HCl_3 , P , Ga , low temp.	hi ρ	--	--
	$AsCl_3$, PH_3 , Ga	hi ρ	--	--

TABLE IV

Electrical Properties of Epitaxial GaP

Sample Number and Orientation	Deposition Temperature (°C)	Electrical Properties			Notes
		Resistivity	Mobility	Carrier Conc.	
AP138-3<111>A	840	hiρ	---	-----	(a)
-3<111>B	"	0.38	130	1.3×10^{17}	
-5<111>A	817	hiρ	---	-----	
-5<111>B	"	0.78	145	6×10^{16}	
-6<111>A	806	hiρ	---	-----	
-6<111>B	"	0.58	155	7×10^{16}	
-8<111>A	789	hiρ	---	-----	
-8<111>B	"	0.64	160	6×10^{16}	
-9<111>A	778	hiρ	---	-----	
-9<111>B	"	1.0	160	4×10^{16}	
SC92-2<111>B	832	2.6-0.6	80-190	$3-5 \times 10^{16}$	(b)
-3<111>B	800	25	95	3×10^{15}	
SC94-3<111>B	830	0.36	170	1.0×10^{17}	(c)
-5<111>B	804	1.4	150	3×10^{16}	
-7<111>B	775	5.0	140	9×10^{15}	
SC93-1<211>A	858	hiρ	---	-----	(d)
-1<211>B	"	14	85	5×10^{15}	
-3<100>	827	hiρ	---	-----	
-6<111>A	788	hiρ	---	-----	
-6<111>B	"	4	165	1.5×10^{16}	
SC91-3<100>	841	53 - hiρ	105 - hiρ	1.1×10^{15} - hiρ	(e)
-6<111>B	810	3.7	75	2.2×10^{16}	

TABLE IV

(continued)

Electrical Properties of Epitaxial GaP

(a) C_2HCl_3 , P , Ga system.

(b) $AsCl_3$, P , Ga system, wafers supported at 30° to flow on BN plates. Deposit polycrystalline.

(c) $AsCl_3$, P , Ga system, pair of wafers back to back at each position.

(d) $AsCl_3$, PH_3 , Ga system.

(e) $AsCl_3$, P , Ga system, $GaAs_{(1-x)}P_x$ alloy. <100>, $x = 0.605$; <111>B, $x = 0.565$.

TABLE VI

Emission Spectroscopic Analysis of Epitaxial GaP

Sample Number and Orientation	Impurity Concentration (ppm)					Elect. Carrier Conc.	Systems, Notes
	Si	Ca	Mg	Ag	Other		
SC65-6<100>	<0.1	~0.5	0.25	<0.1		(2×10^{14})?	PCl_3, Ga, low temp.
SC86-4<111>A	<0.1	~0.5	<0.1	<0.1		(7×10^{13})?	C_2HCl_3, P, Ga, med. temp.
SC86-4<111>B	~0.1	~0.5	0.1	----	≤0.1 Tl	9.8×10^{15}	"
SC88-3<100>	~0.5	~0.5	0.25	----	~0.2 Pt <0.1 Ti <0.1 V	1.1×10^{16} p	C_2HCl_3, P, Ga, high temp.
SC90-1<211>B	~0.1	~0.5	0.15	---		2.9×10^{15}	C_2HCl_3, P, Ga, low temp.
SC90-3<100>	~0.1	~0.5	0.2	---		6×10^{13}	"
SC90-6<111>B	~0.1	0.7	0.15	---		7.4×10^{16}	"
SC76-4<111>B	1.4	0.2	0.15	<0.1		$\sim6 \times 10^{16}$	$AsCl_3$, P, Ga
SC77-4<111>B	0.5	1~2	0.5	<0.1		2.9×10^{16}	"
SC78-4<100>	<0.1	~0.5	0.3	<0.1		$<5.2 \times 10^{14}$	"
SC87-4<100>	0.3	~0.5	0.4	---		1.9×10^{16} Te	"
SC93-3<100>	<0.1	~0.1	<0.1	~1		hi ρ	$AsCl_3$, PH_3, Ga
SC93-6<111>B	~0.1	0.5	0.11	<0.1		1.5×10^{16}	"
SC68-2<211>	0.2	~0.5	0.4	≤0.1		hi ρ	H_2O, GaP

All samples contained Cu and Al, reported at <0.1 ppm.

TABLE VII

Solar Cell Evaluation

GaP Solar Cells

(Magnesium Diffusion)

Run No.	Slice No.	P Diffusant & Amount	Diffusant Temp(°)	Diffusion Time	V_{oc}* (volts)	J_{sc}* (ma/cm^2)	Spectral Response Peak (microns)	Cell Area (cm^2)	β, Temp. ± Coeff. V_{oc} (mv/deg)	V_{oc} ± at 350° (volts)
NA73	SC78-2	2.5mgMg. 2.1mgP	1000	16h.	.83	.03	.53	.09	2.2	.0+
NA73	SC88-6<111>B	"	"	"	Sample Broke		---	.03	---	---
NA73	SC89-7<111>B	"	"	"	.13	.00	---	.12	---	---

* measured in sunlight

± measured using tengsten source

TABLE VIII

Compilation of Hall Effect, Resistivity, Solar Cell Characteristics, Emission Analysis,

Electroluminescence Data for GaP Samples SC90-6, SC77-4, SC76-4

Characteristics	SC90-6	Sample SC77-4	SC76-4
(a) Hall Resistivity Data:			
Conductivity Type	N	N	N
Donor Concentration, N_D	1.2×10^{17}	2.2×10^{16}	4.2×10^{16}
Acceptor Concentration, N_A	8.4×10^{14}	8.9×10^{15}	2.6×10^{16}
Total Ionized Conc., N_I	1.2×10^{17}	3.1×10^{16}	6.8×10^{16}
Donor Impurity Ionization Energy ΔE_D (ev)	.114	.085	.087
Hall Mobility, R/ρ, Temperature Relationship	$R/\rho \propto T^{-1.95}$	$R/\rho \propto T^{-1.9}$	$R/\rho \propto T^{-1.88}$
Carrier Conc. at R. T., $n_{R. T.}$	5.8×10^{16}	1.33×10^{16}	1.6×10^{16}
Mobility at R. T., $\mu_{R. T.}$ (cm^2/volt sec)	139	146	125
(b) Solar Cell Characteristics:			
Conversion Efficiency (%)	1.2	1.9	1.5
V_{oc} at R. T. (volts)	1.21	1.38	1.40
J_{sc} at R. T. (ma/cm^2)	1.41	1.60	1.43
V_{oc} at 350°C (volts)	.30	.42	.45
J_{sc} at 350°C (ma/cm^2)	1.07	1.51	1.36

TABLE VIII

(continued)

Compilation of Hall Effect, Resistivity, Solar Cell Characteristics, Emission Analysis, Electroluminescence Data for GaP Samples SC90-6, SC77-4, SC76-4

		Sample	
Characteristics	SC90-6	SC77-4	SC76-4
(c) Emission Analysis:			
Impurities			
Silicon (PPM)	~0.1 (9×10^5 atoms/cm^3)	0.5 (4.5×10^{16} atoms/cm^3)	1.4 (1.25×10^{17} atoms/cm^3)
Magnesium (PPM)	0.15 (1.6×10^{16})	0.5 (5×10^{16})	0.15 (1.6×10^{16})
Cu (PPM)	<0.1	<0.1	<0.1
Ag (PPM)	---	<0.1	<0.1
Pt (PPM)	---	---	---
Ti (PPM)	---	---	---
V (PPM)	---	---	---
Al (PPM)	0.1	<0.1	<0.1
Ca (PPM)	0.7 (4.6×10^{16})	1~2 ($.64$-1.2×10^{17})	0.2 (1.3×10^{16})
Te (PPM)	---	---	---
(d) Electroluminescence Data:			
green/red ratio	<1*	1.5	.5

* qualitative value, quantitative result not available yet

TABLE IX

GaP Solar Cell Evaluation for Final Quarter

Run No.	Slice No.	Orientation	V_{oc}[†] (volts)	J_{sc}[†] (ma/cm²)	Spectral Response Peak (microns)	Cell Area (cm²)	β, Temp.[‡] Coefficient of V_{oc}(mv/deg)	V_{oc}[‡] at 350°C (volts)	Conversion[‡] Efficiency (%)
NA72	SC88-6	<111>B	1.32	1.07	.445	.56	2.4	.39	- - -
NA72	SC8907	<111>B	.98	.76	.45	.83	2.0	.18	- - -
NA72	SC89-3	<100>	.85	.27	.46,.52	.75	3.4	.10	- - -
NA72	SC90-6	<111>B	1.21	1.41	.45	.17	3	.30	1.2
NA72	SC78-2	<111>B	.83	.03	.53	.09	2.2	.04	- - -
NA73	SC88-6	<111>B	Sample Broke			.03	- - -	- - -	- - -
NA73	SC89-7	<111>B	.13	.00	- - -	.12	- - -	- - -	- - -
NA74	SC74-2		.74	.01	.45	.16	- - -	- - -	- - -
NA74	SC74-4		.13	- - - -	- - - -	.10	- - -	- - -	- - -
NA74	AP138-5	<111>B	.93	.01	.45,.525 .7 (broad)	.07	4.7	.03	- - -
NA76	SC93-6	<111>B	1.20	1.12	.475	.39	2.5	.36	.46
NA76	SC93-3	<100>	1.28	.23	.50	.34	- - -	.01	- - -
NA76	SC93-6	<111>A	.02	.00	- - -	.90	- - -	- - -	- - -
NA77	SC92-2	<111>B	.94	.53	.45,.525	.44	- - -	- - -	- - -
NA77	SC92-3	<111>B	.97	.80	.525,.45	.75	- - -	- - -	- - -
NA77	SC94-3	<111>B	.94	.37	.45	.44	- - -	- - -	- - -
NA77	SC94-5	<111>B	.85	.84	.45	1.38	- - -	- - -	- - -
NA77	SC94-7	<111>B	1.38	.64	.46	.81	3.5	.44	- - -

† measured in sunlight
‡ measured in sunlight, intensity of 82 mw/cm²
± measured using tungsten source

TABLE X

Evaluation of $GaAs_{1-x}P_x$ Solar Cells

Run No.	Slice No.	Alloy Composition	n no/cm³	V_{oc}* (volts)	J_{sc}* ma/cm²	Spectral Response Peak (microns)	Cell Area cm²	$V_{oc}^{\pm}$ at 250°C (volts)	$J_{sc}^{\pm}$ at 250°C (ma/cm²)	Conversion Efficiency %
10	G1080	GaAs	10^{17}	.84	10	---	1.39	---	---	6%
75	AP91-4	$GaAs_{.88}P_{.12}$	5×10^{16}	.28	3.3	.77	.42	.05	.71	---
75	AP122-3	$GaAs_{.86}P_{.14}$	2×10^{17}	.07	1.4	.72	.36	---	---	---
75	AP132-3	$GaAs_{.85}P_{.15}$	2×10^{17}	.14	1.48	.70	.64	---	---	---
71	203B	$GaAs_{.60}P_{.40}$	1×10^{17}	.46	1.06	.625	.15	.18	1.7	---
71	334B	$GaAs_{.48}P_{.52}$	6×10^{17}	.11	1.00	.585	.164	.05	1	---
75	SC91-6	$GaAs_{.43}P_{.57}$	3×10^{16}	1.13	1.64	.57	.14	.54	2.2	1.3%
75	SC91-3	$GaAs_{.39}P_{.61}$	1×10^{15}	1.18	1.1	.56	.27	.55	1.8	---
71	174Te	$GaAs_{.25}P_{.75}$	9×10^{17}	.73	.51	.505	.085	.28	.71	---
71	891	$GaAs_{.16}P_{.84}$	1×10^{18}	.22	.09	.495	.16	.02	.08	---

* measured in sunlight

± measured using tungsten source (100 mw/cm²)

TABLE XI

Samples Submitted to NASA

Sample No. & Orientation	System and Notes	Electrical		Solar Cell Characteristics					
		n	μ	V_{oc} (volts)	J_{sc} (ma/cm²)	Response Peak (μ)	Area (cm²)	V_{oc} 350° (volts)	Eff. %
SC55-7<111>B	HCl, P, Ga	7.6×10^{17}	190	--	...	--	--	--	--
545814<100>	Close-space	1.1×10^{17}	75	--	--	--	--	--	--
SC57-3<100>	PCl₃, Ga, low temp.	5×10^{13} (∵) (800)(?)	--	--	--	--	--	--	--
SC58-6<111>B	PCl₃, Ga, low temp.	4.3×10^{16}	135	--	--	--	--	--	--
SC60-3<111>B	PCl₃, Ga, high temp.	$1.8 \times 10^{17}(?)(600)(?)$	--	--	--	--	--	--	--
SC60-7<111>A	PCl₃, Ga, high temp.	6×10^{14}	120	--	--	--	--	--	--
NA57 SC62-3<111>B	PCl₃, Ga, low temp.	$<1.6 \times 10^{17}$	96	--	--	--	--	--	--
NA57 SC64-3<111>B	PCl₃, Ga, low temp.	$<2.7 \times 10^{17}$	150	--	--	--	--	--	--
NA59 SC68-5<100>	H₂O, GaP	hi ρ	---	1.17	0.02	0.51	0.42	--	--
NA59 SC68-8<111>B	H₂O, GaP	hi ρ	---	1.20	0.20	0.46	0.52	--	--
NA63 SC73-4<111>B	H₂O, P, Ga, Te doping	4.9×10^{16}	160	1.18	1.52	--	0.21	--	1.0
NA63 SC75-4<100>	AsCl₃, P, Ga	$\leq 10^{14}$	---	1.06	0.028	--	0.71	--	--
NA65 SC77-2<111>B	AsCl₃, P, Ga	6.2×10^{16}	160	1.28	--	--	1.26	--	--
NA65 SC78-2<100>	AsCl₃, P, Ga	6×10^{15}	120	0.56	--	--	1.30	--	--
NA69 SC86-2<111>B	C₂HCl₃, P, Ga, med. temp.	1.6×10^{17}	114	1.39	1.43	0.445	1.04	--	1.5
NA69 SC87-2<100>	AsCl₃, P, Ga, Te doping BN tube liner	1.7×10^{16}	110	0.29	0.003	0.54 (neg)	1.25	--	--

TABLE XI

(continued)

Samples Submitted to NASA

Sample No. & Orientation	System and Notes	Electrical		V_{oc} (volts)	J_{sc} (ma/cm²)	Solar Cell Characteristics			V_{oc} 350° (volts)	Eff. %
		n	μ			Response Peak (μ)	Area (cm²)			
NA72 SC88-6<111>B	C_2HCl_3, P, Ga, high temp.	4.4×10^{16}	150	1.32	1.07	0.445	0.56		0.39	1.0
NA72 SC89-7<111>B	C_2HCl_3, P, Ga, low temp.	2.6×10^{16}	120	0.98	0.76	0.45	0.83		0.18	--
NA75 SC91-3<100>	GaAs.39P.61 alloy AsCl_3, P, Ga	$<1 \times 10^{15}$	100	1.18	1.1	0.56	0.27		--	--
NA75 AP91-4<100>	GaAs.88P.12 alloy 9μ layer	5.2×10^{16}	2400	0.28	3.3	0.77	0.42		--	--
NA76 SC93-3<100>	$AsCl_3$, PH_3, Ga	hi ρ	--	1.28	0.23	0.50	0.34		0.01	--
NA76 SC93-6<111>A	$AsCl_3$, PH_3, Ga	hi ρ	--	0.02	0.001	--	0.91		--	--
NA77 SC92-2<111>B	$AsCl_3$, P, Ga, poly.	4×10^{16}	80	0.94	0.53	0.45, 0.53	0.19		--	--
NA77 SC94-5<111>B	$AsCl_3$, P, Ga, poly.	3×10^{16}	155	0.85	0.84	0.45	0.87		--	--

LIST OF FIGURES

TABLE V

Electrical Properties of Doped, Vapor Grown, Epitaxial GaP Crystals

Sample Number and Orientation	System	Gas Doping Concentration (atoms/cm³ GaP)	Electrical Properties			Ratio Gas Dop. Conc. to Carrier Conc.
			Resistivity	Mobility	Carrier Conc.	
SC71-3<100>	H_2O , P , Ga	4.4×10^{16} Te	hi ρ	---	---	>100
-6<111>B			130	63	7.6×10^{14}	58
SC72-2<100>	H_2O (high initial pressure), P , Ga	2.7×10^{18} Te	0.68	49	1.9×10^{17}	14
-4<100>			0.28	69	3.2×10^{17}	8.4
-6<100>			0.22	58	5.0×10^{17}	5.4
SC73-2<111>B	H_2O , P , Ga	1.6×10^{18} Te	1.4	145	3.0×10^{16}	53
-4<111>B			0.80	160	4.9×10^{16}	33
-6<111>B			0.56	130	8.4×10^{16}	19
SC74-2<111>B	H_2O , P , Ga	1.5×10^{19} Te	>0.12	<84	$<6 \times 10^{17}$	25
-4<111>B			0.083	103	7.3×10^{17}	21
SC80-2<100>	$AsCl_3$, P , Ga	1.2×10^{17} Te	67	150	6.4×10^{14}	190
-4<100>			55	120	9.2×10^{14}	130
SC81-2<111>B	$AsCl_3$, GaP (6-15 ppm Te) , BN tube liner	$1.2\text{-}2.9 \times 10^{17}$ Te	0.16	58	6.9×10^{17}*	0.29
-4<111>B			0.20	56	5.7×10^{17}*	0.35
-6<111>B			0.24	46	5.7×10^{17}*	0.35
SC82-2<111>B	$AsCl_3$, GaP (6-15 ppm Te)	$1.2\text{-}2.9 \times 10^{17}$ Te	0.16	69	5.8×10^{17}*	0.34
-4<111>B			0.09	79	8.6×10^{17}*	0.23

TABLE V
(continued)

Electrical Properties of Doped, Vapor Grown, Epitaxial GaP Crystals

Sample Number and Orientation	System	Gas Doping Concentration (atoms/cm³ GaP)	Electrical Properties			Ratio Gas Dop. Conc. to Carrier Conc.
			Resistivity	Mobility	Carrier Conc.	
SC83-2<111>A	AsCl$_3$, P, Ga	2.9 x 10^{18} Te	0.026-12	104-77	2.4 x 10^{18} - 6.8 x 10^{15}	1.2-430
<111>B			0.007-0.08	101-86	8.8 x 10^{18} - 8.8 x 10^{17}	0.33-3.3
-4<111>A			7.5	90	9.3 x 10^{15}	310
<111>B			0.11	80	7.0 x 10^{17}	4.1
SC87-2<100>	AsCl$_3$, P, Ga BN tube liner	3.2 x 10^{18} Te	3.2	110	1.7 x 10^{16}	190
-4<100>			2.9	115	1.9 x 10^{16}	
-6<100>			2.9	135	1.6 x 10^{16}	
AP139-1<211>A	AsCl$_3$, PH$_3$, Ga	1.1 x 10^{20} Sn	0.044	61	2.3 x 10^{18}	48
<211>B			0.098	46	1.4 x 10^{18}	79
-3<111>A			0.055	99	1.1 x 10^{18}	100
<111>B			0.5	23	4 x 10^{17}	270
-5<100>			0.060	89	1.2 x 10^{18}	92
-6<100>			0.08	100	8 x 10^{17}	140
-7<111>A			0.07	92	1.0 x 10^{18}	110
-7<111>B			0.05	18	7 x 10^{17}	160

* Polycrystalline

LIST OF FIGURES

Figure 1

AP139-5<100> , heavily Sn doped, showing inhomogeneous
distribution of Sn. Sample polished on both
sides, photographed with diffused, trans-
mitted light.

Figure 2

SC89-1 Thick GaP deposits grown on each side of vertically supported substrate. Top <211>A , bottom <211>B .
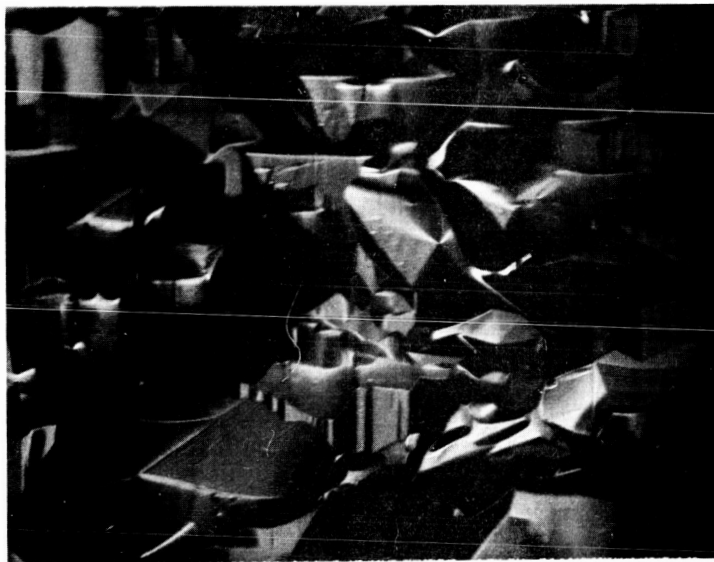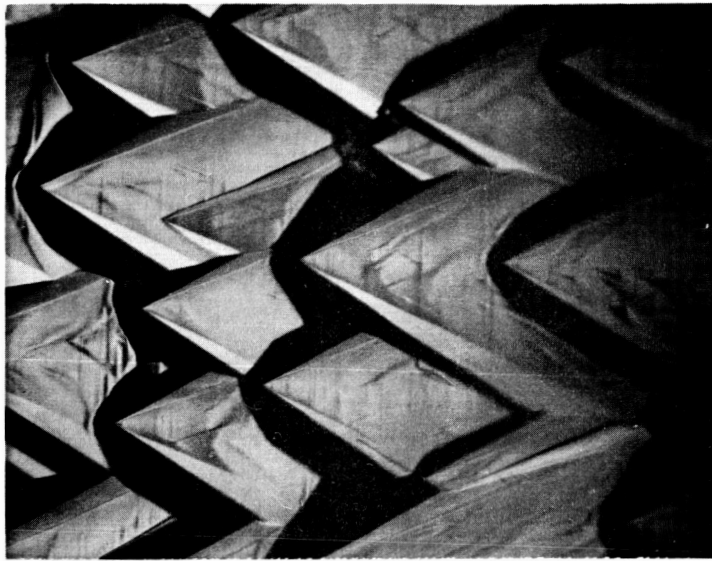
Figure 3

SC89-1 <211>A (top) and <211>B (bottom) <110> direction
horizontal A to left, B to right. Dark field
illumination ~100X .
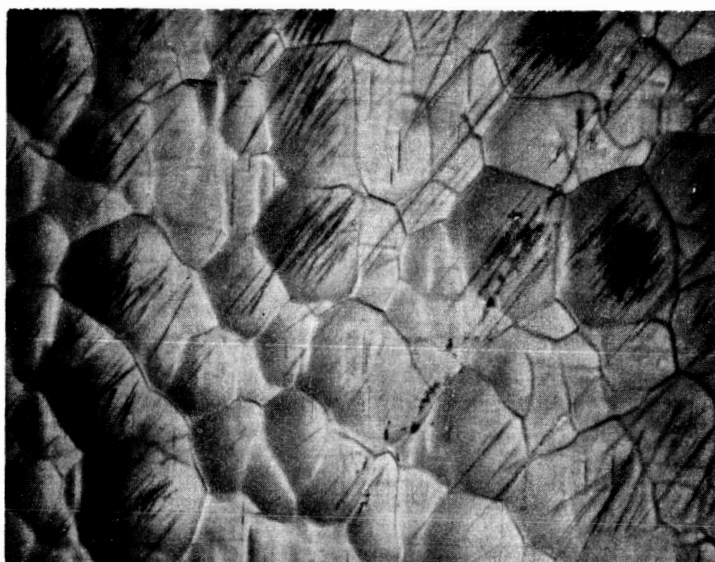
Figure 4

AP139-1 <211>A (top) and <211>B (bottom), showing effect
         of heavy Sn doping.   Orientation same as in Figure
         3. Bright field illumination. Surfaces have been
         scratched. 50X .
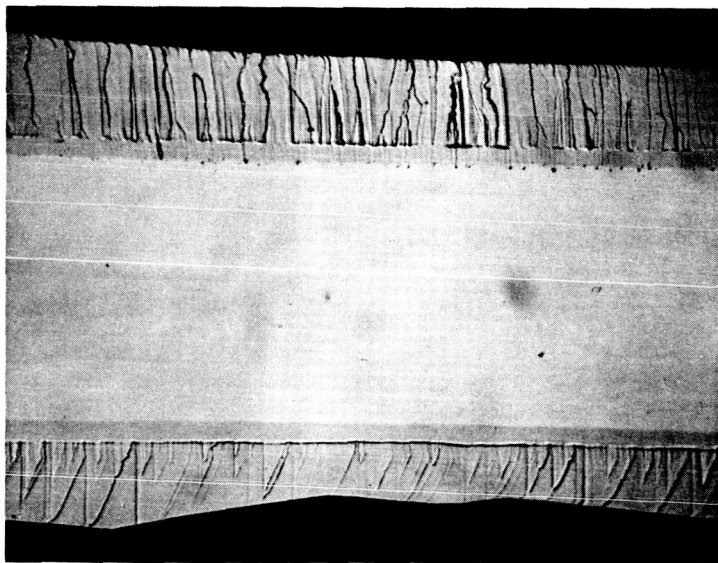
Figure 5

SC83-2<111>, cleaved section. Te doped epitaxial GaP
deposit on both sides of GaAs substrate,
A surface at top. 100X.
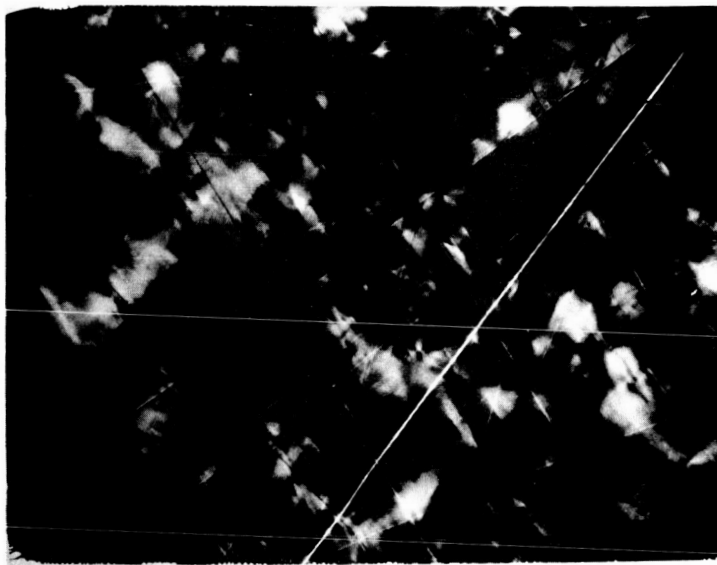
Figure 6

SC90-6<111>A , annealed and polished, strain birefringence
shown by transmission using crossed
polarizers. 100X .
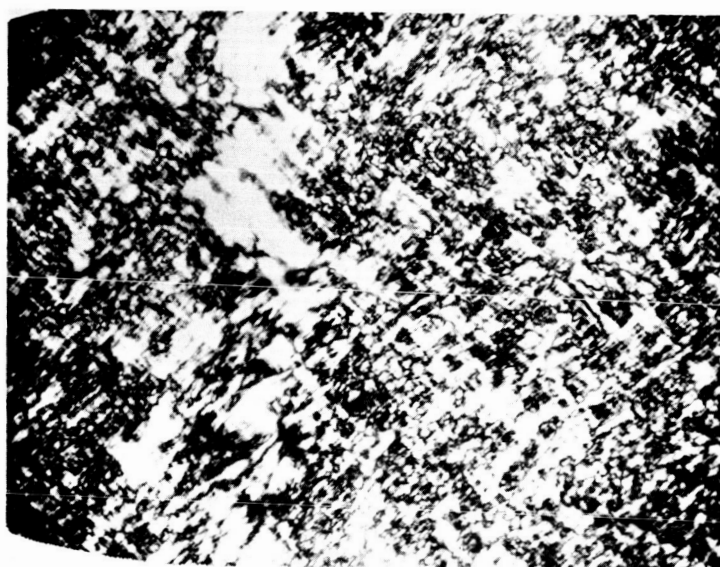
Figure 7

SC94-7<111>B , same conditions as Figure 6.   100X .
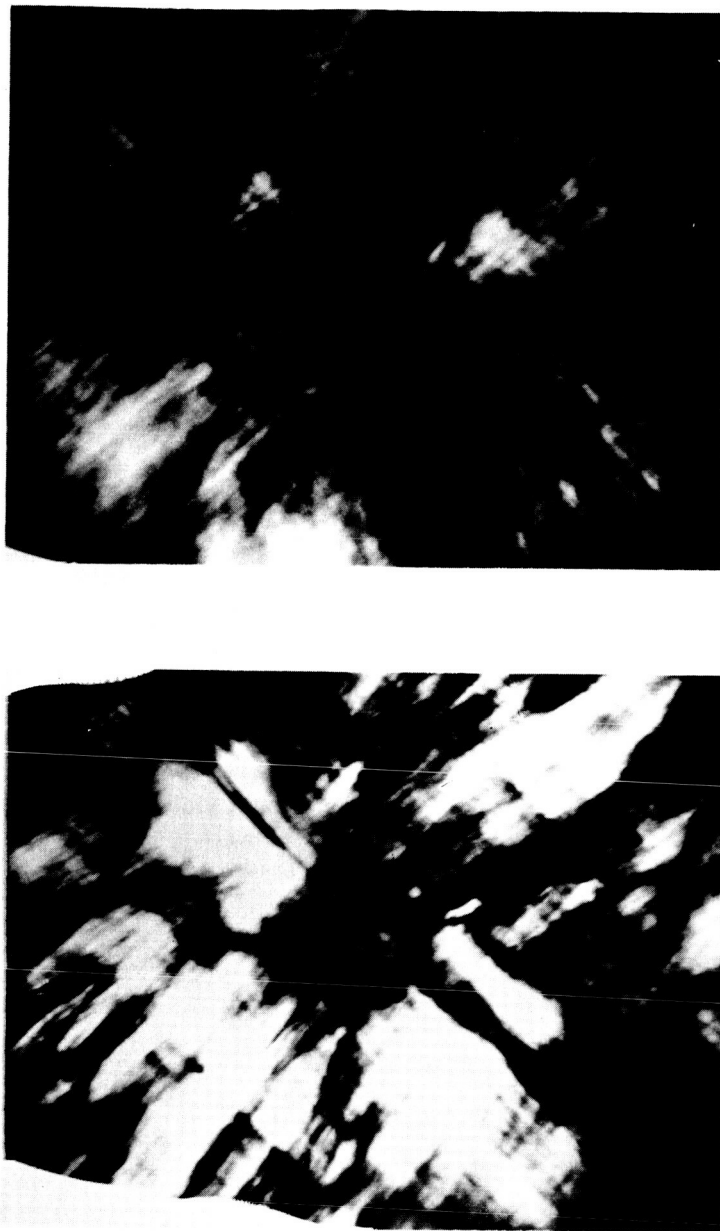
Figure 8

AP139-5<100> , in region of stacking fault array at center
of bump. (Top) same conditions as
Figures 6 and 7 except exposure time
reduced by factor of 4. (Bottom) rotated
45° . Both 100X .
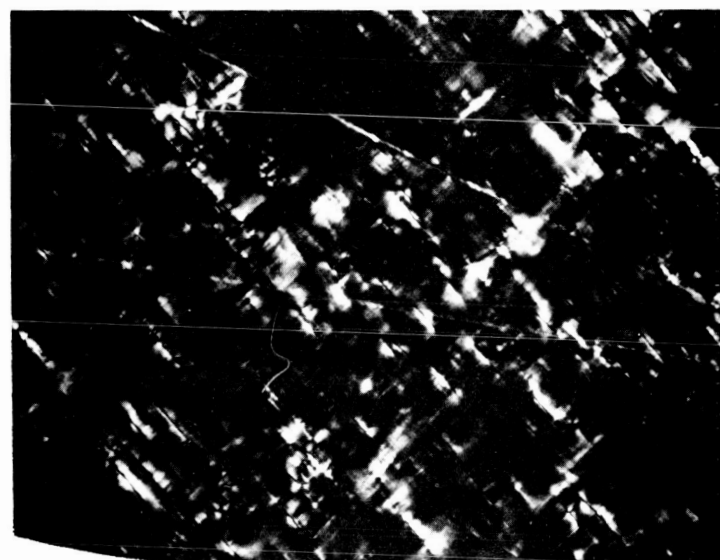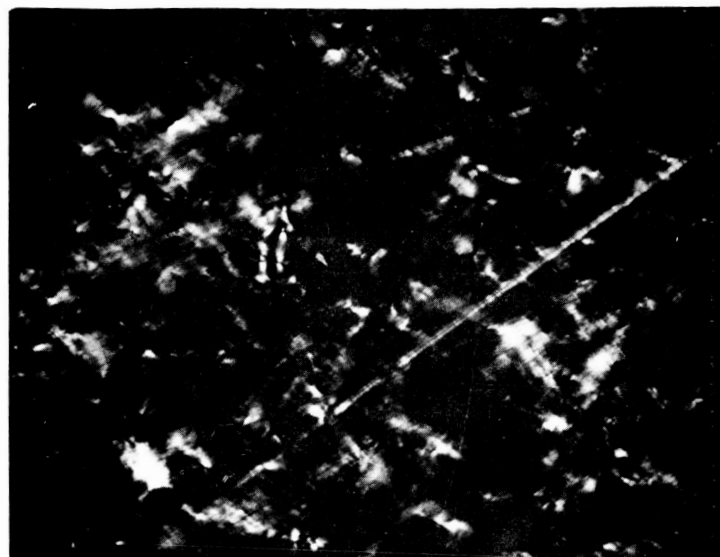
Figure 9

SC93-1<211>A Same conditions as Figures 6 and 7.
Bottom rotated 45° . 100X .

Figure 10

SC90-6<111>A , mechanically polished (3 μ diamond), etched
3 hours in saturated solution of I_2 in
methanol with trace of Br_2 , showing
stacking fault structure. Large black spots
are bottoms of original surface pits not
completely removed on polishing. (Top)
<111>A surface. (Bottom) opposite <111>B
surface. Both 100X .
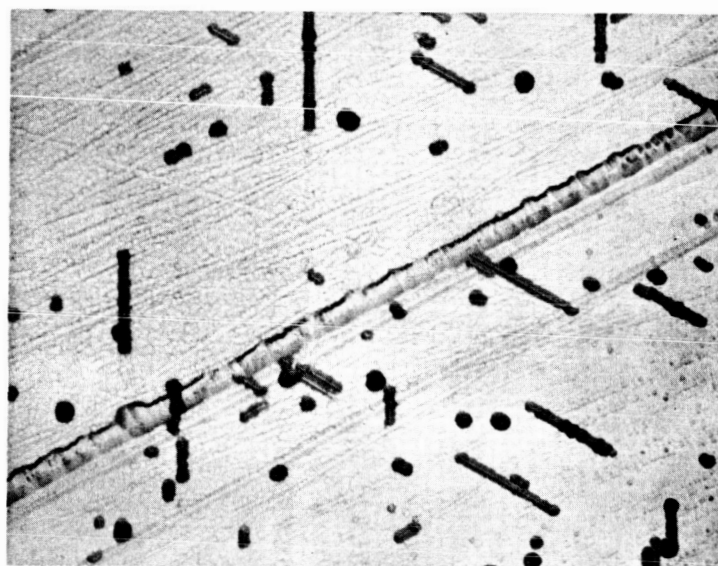
Figure 11

SC90-6<111>A Same as Figure 10.   500X .
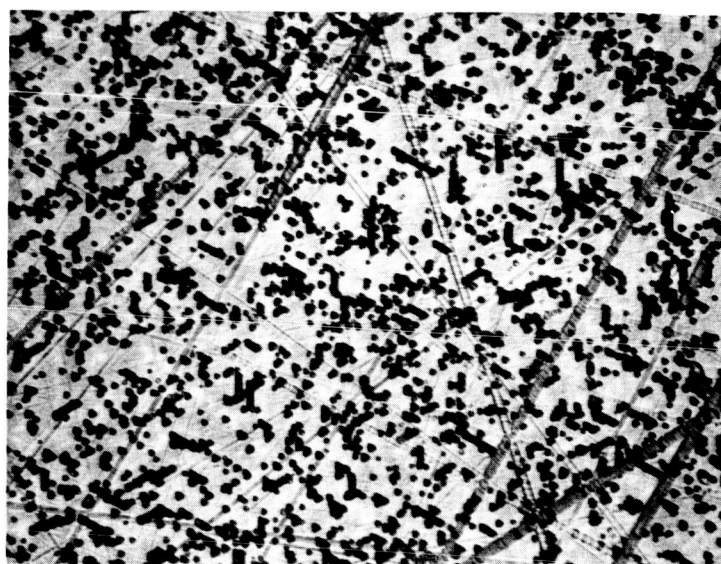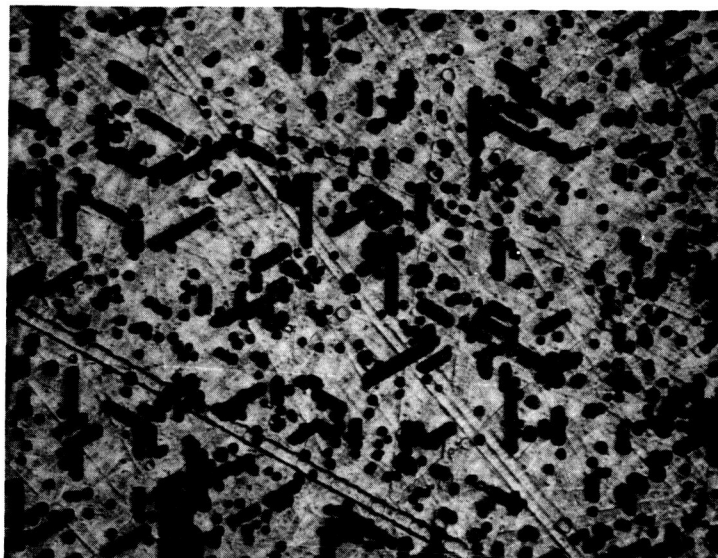
Figure 12

SC90-6<111>A Same area as shown in Figure 10 after
annealing, repolishing and etching 15' in
warm HF-HNO$_3$-AgNO$_3$ etch to reveal
dislocations. (Top) <111>A surface.
(Bottom) opposite <111>B surface. Both 100X .
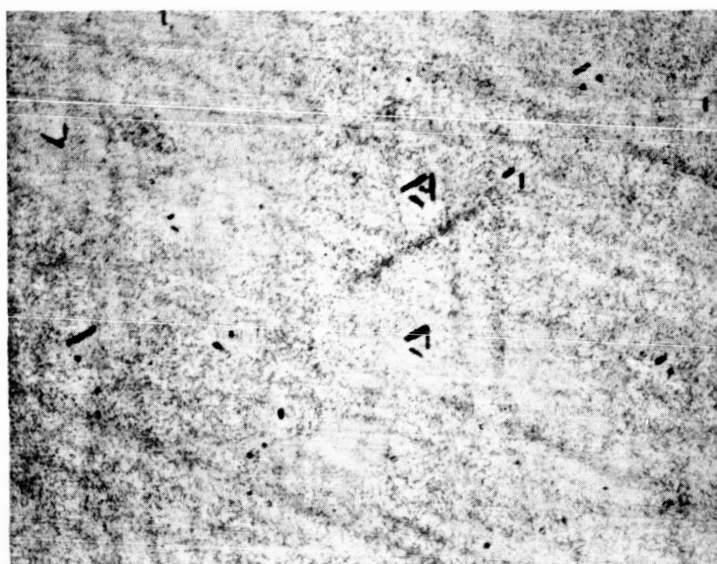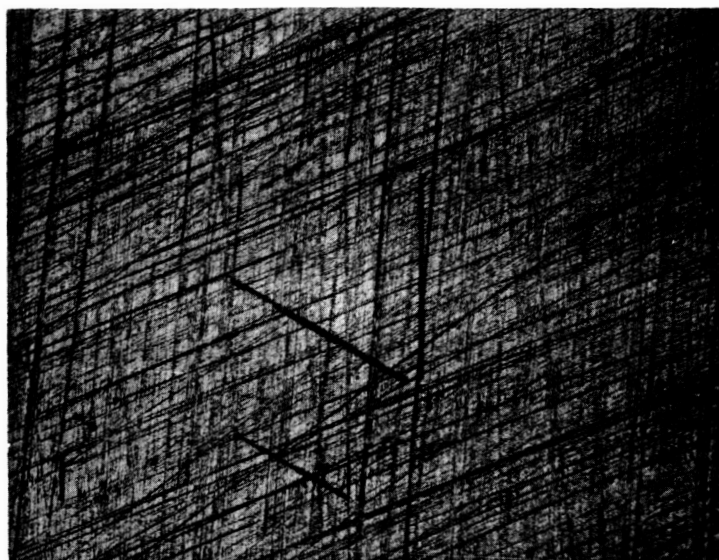
Figure 13

SC94-7<111>B , polished and etched to reveal stacking
faults as in Figure 10. (Top) <111>B
surface. (Bottom) opposite <111>A surface
by transmission. Array of top view faintly
visible. Both 100X .
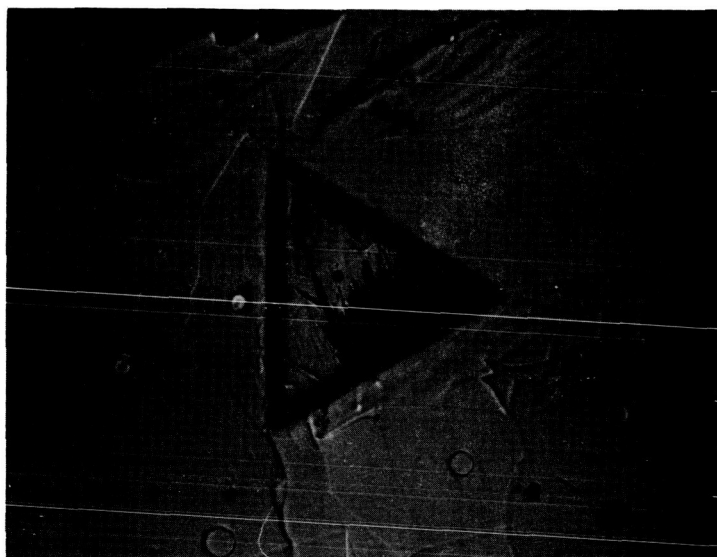
Figure 14

SC94-7<111>B As grown surface after etching in hot HNO_3
to remove substrate, showing triangular
mesa containing stacking fault array.
Surface of mesa is scratched.   50X .
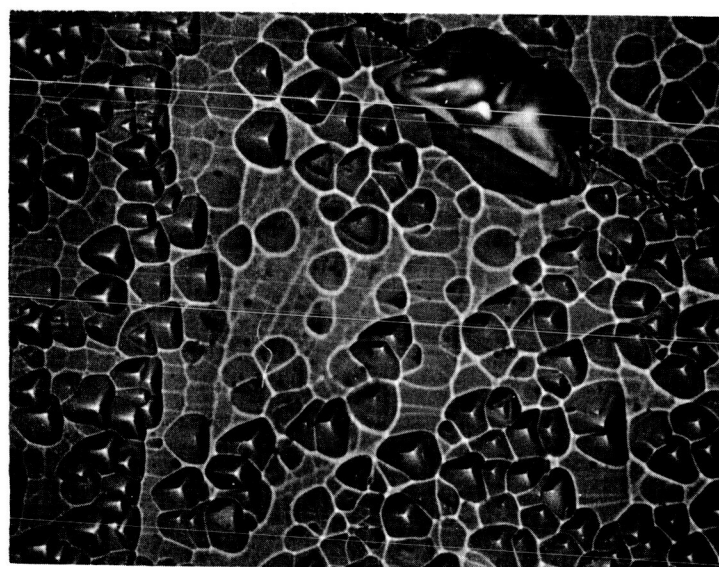
Figure 15

SC94-7<111>B , after treatment described under Figure 12.
(Top) <111>B surface. 100X . (Bottom)
Lower right corner of mesa region. 500X .
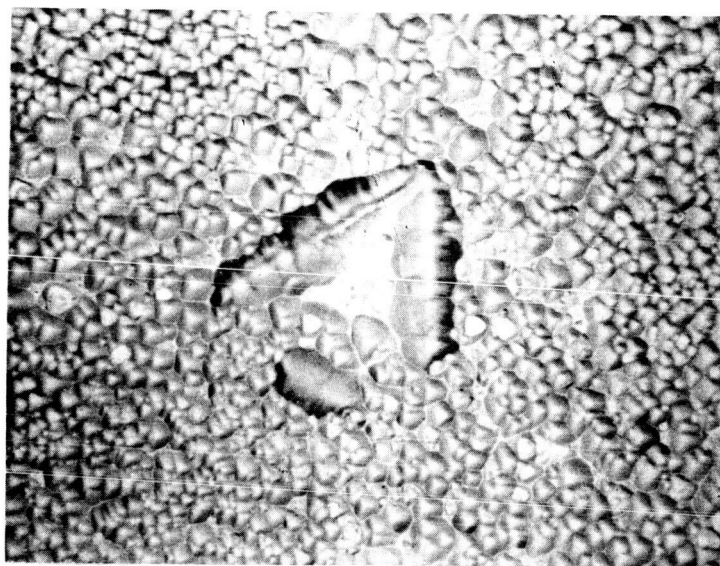
Figure 16

SC94-7<111>B , after same treatment described under
Figure 12. <111>A surface in vicinity
of central stacking fault array. 500X .
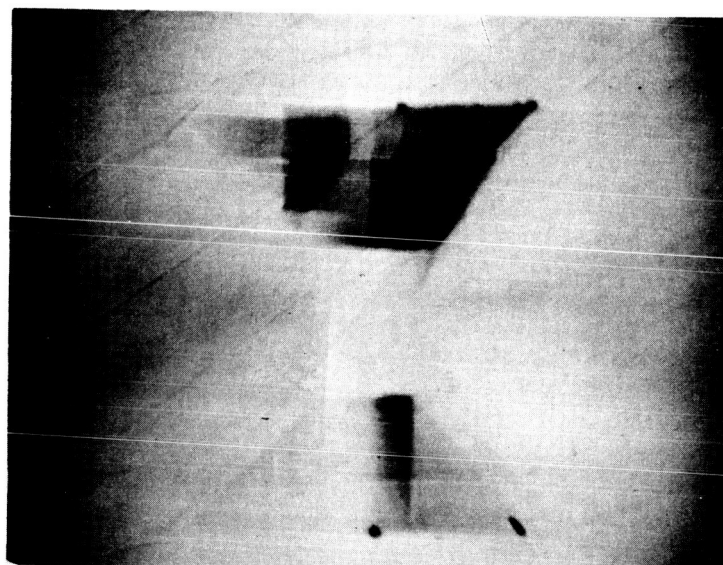
Figure 17

AP139-5<100>, heavily Sn doped, showing lamellar twins
in stacking fault array, by transmission,
focus midway through crystal. 100X .
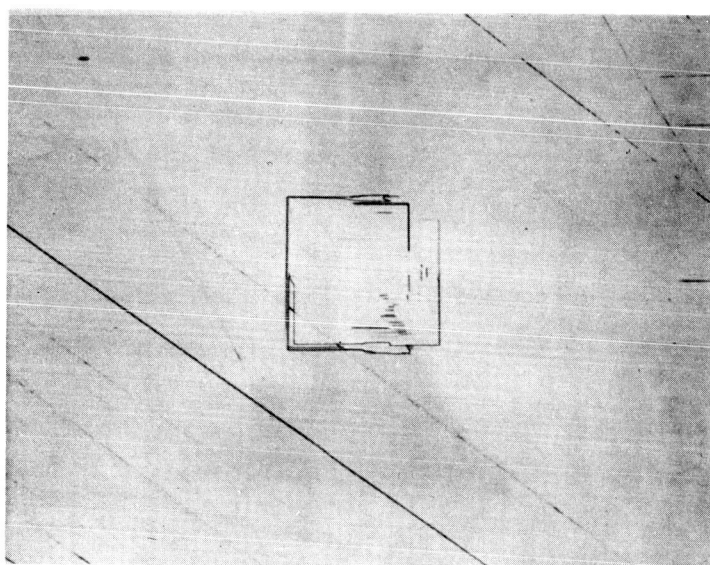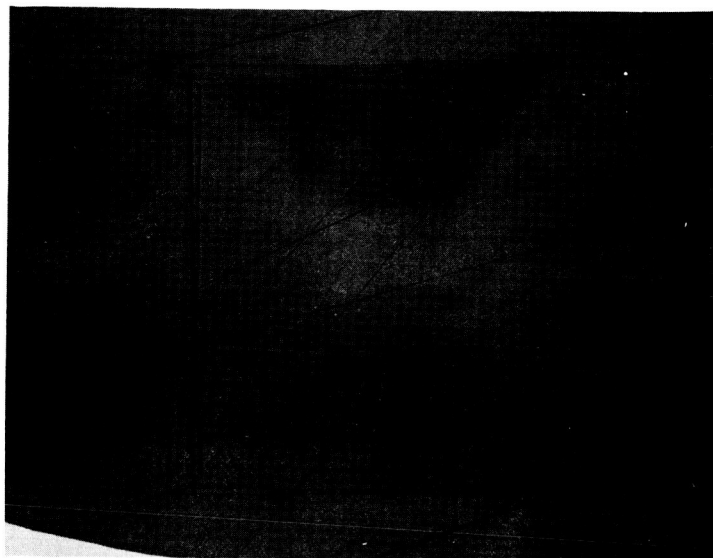
Figure 18

AP139-5<100> Stacking fault and/or lamellar twin array developed by etching in sodium hypochlorite solution, by reflected light. (Top) upper surface. (Bottom) opposite side nearest substrate. Both 100X .
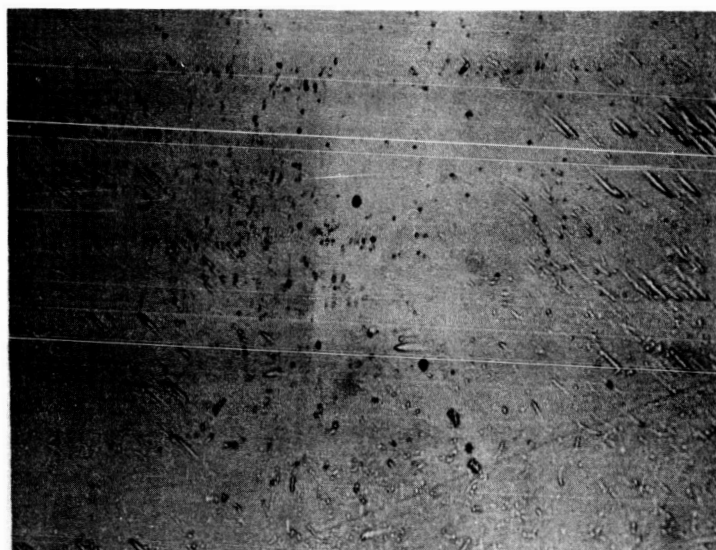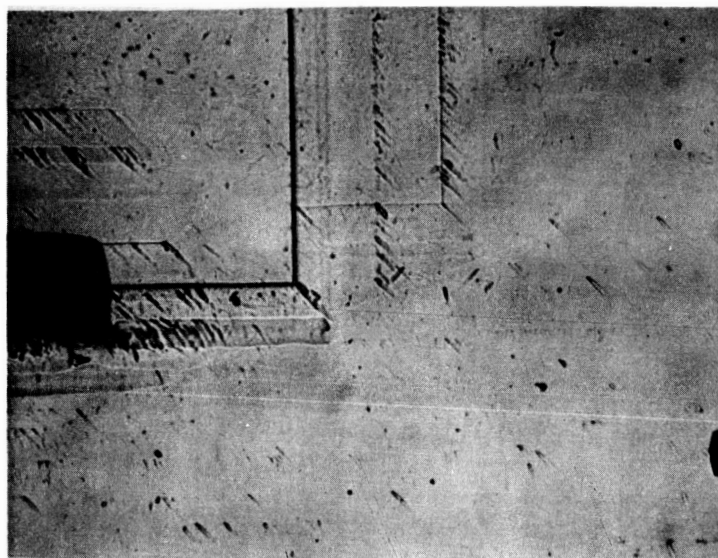
Figure 19

AP139-5<100> Etch pits developed by etching in warm
HF-HNO₃-AgNO₃ after same treatment
as described under Figure 12. (Top)
region near lower right corner of stacking
fault array of Figure 18. (Bottom) area at
boundary between more heavily doped (left)
and less heavily doped (right) regions of
crystal. Both 500X.

Figure 20

SC93-1<211>A , after same treatment as described under
Figure 12. (Top) <211>A surface showing
stacking faults and dislocations. (Bottom)
opposite <211>B surface showing stacking
faults. Both 100X .

Figure 21

Conversion efficiency as a function of solar intensity for GaP solar cells NA68 SC76-4, NA68 SC77-4, NA72 SC90-6, NA76 SC93-6 and for GaAs$_{.43}$P$_{.57}$ cell NA75 SC91-6.

SC 90 - 6 <111>B

Figure 22

Hall effect and resistivity as a function
of temperature for n-type epitaxial GaP
sample SC90-6.

SC 77-4<111>B

Figure 23

Hall effect and resistivity as a function
of temperature for n-type epitaxial GaP
sample SC77-4.

SC 76-4⟨III⟩B

<u>Figure 24</u>

Hall effect and resistivity as a function
of temperature for n-type epitaxial GaP
sample SC76-4.
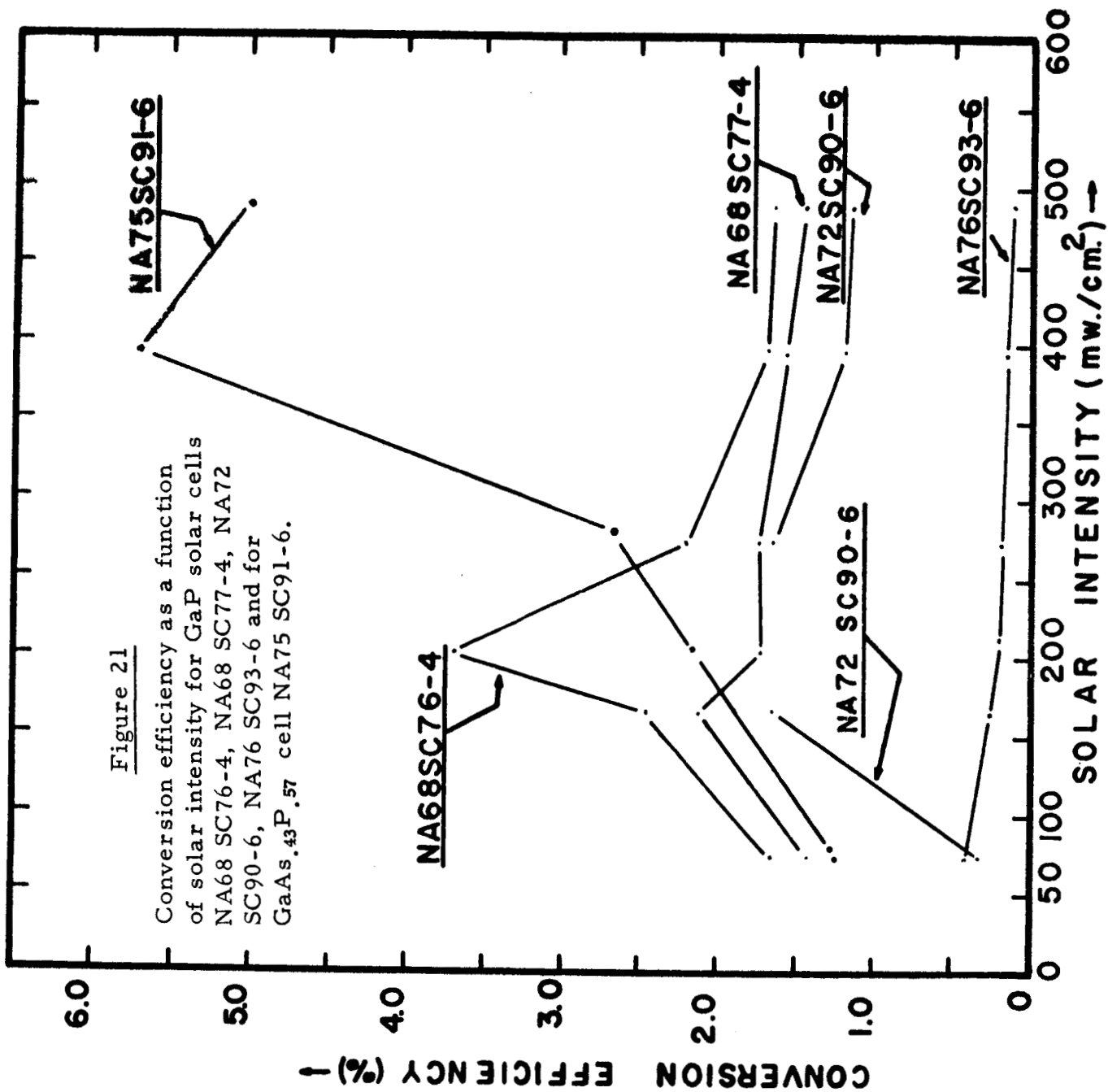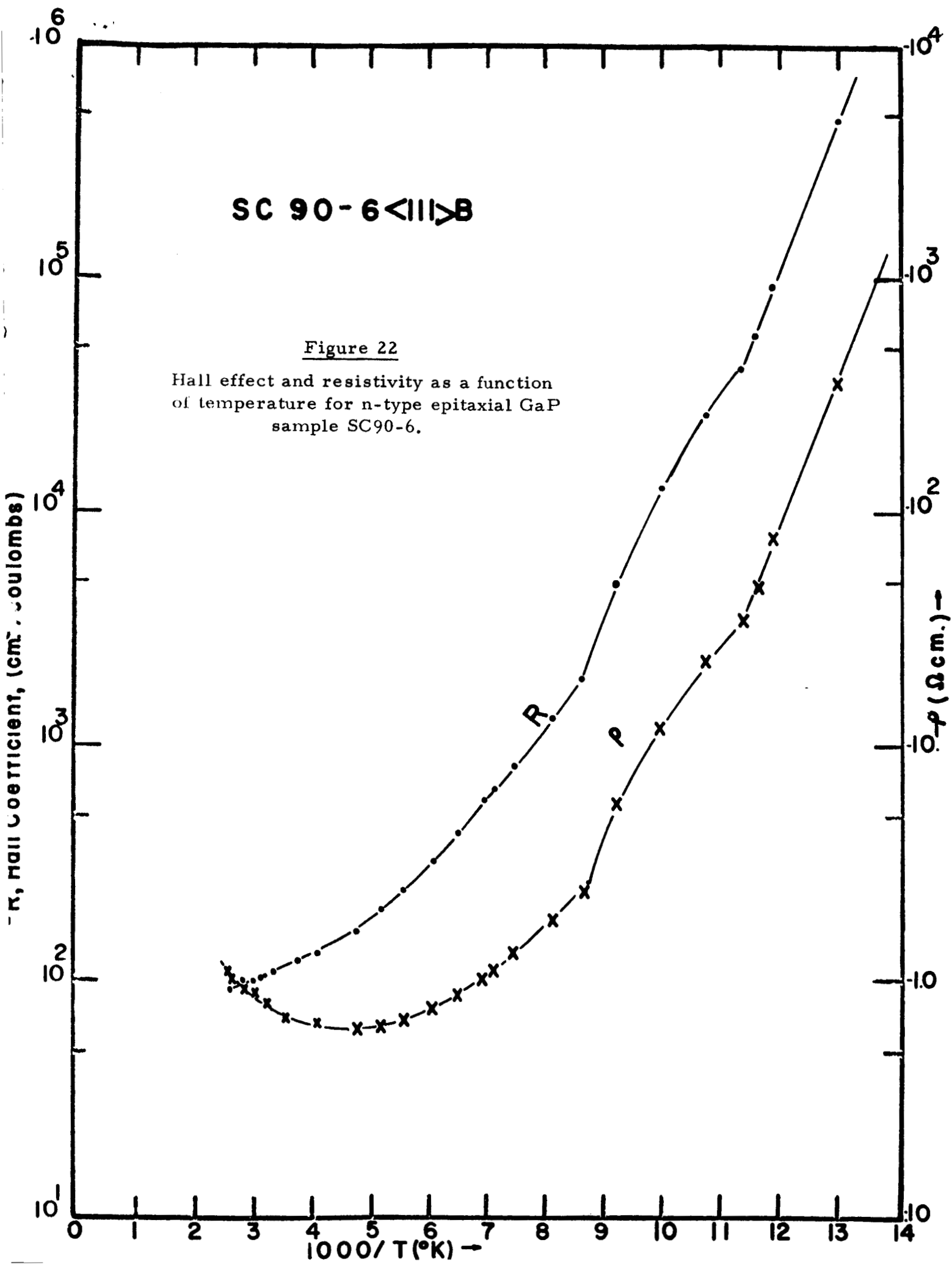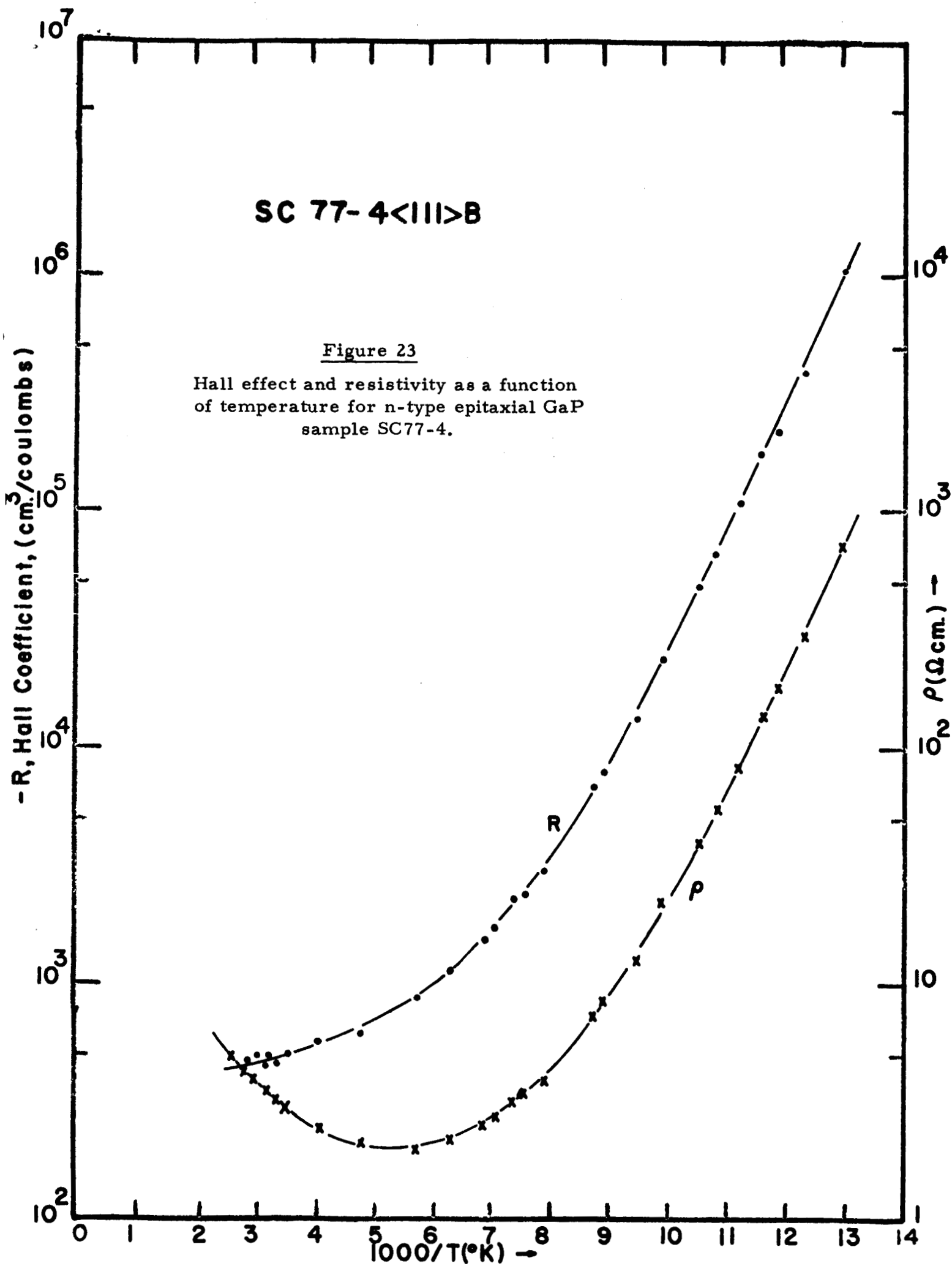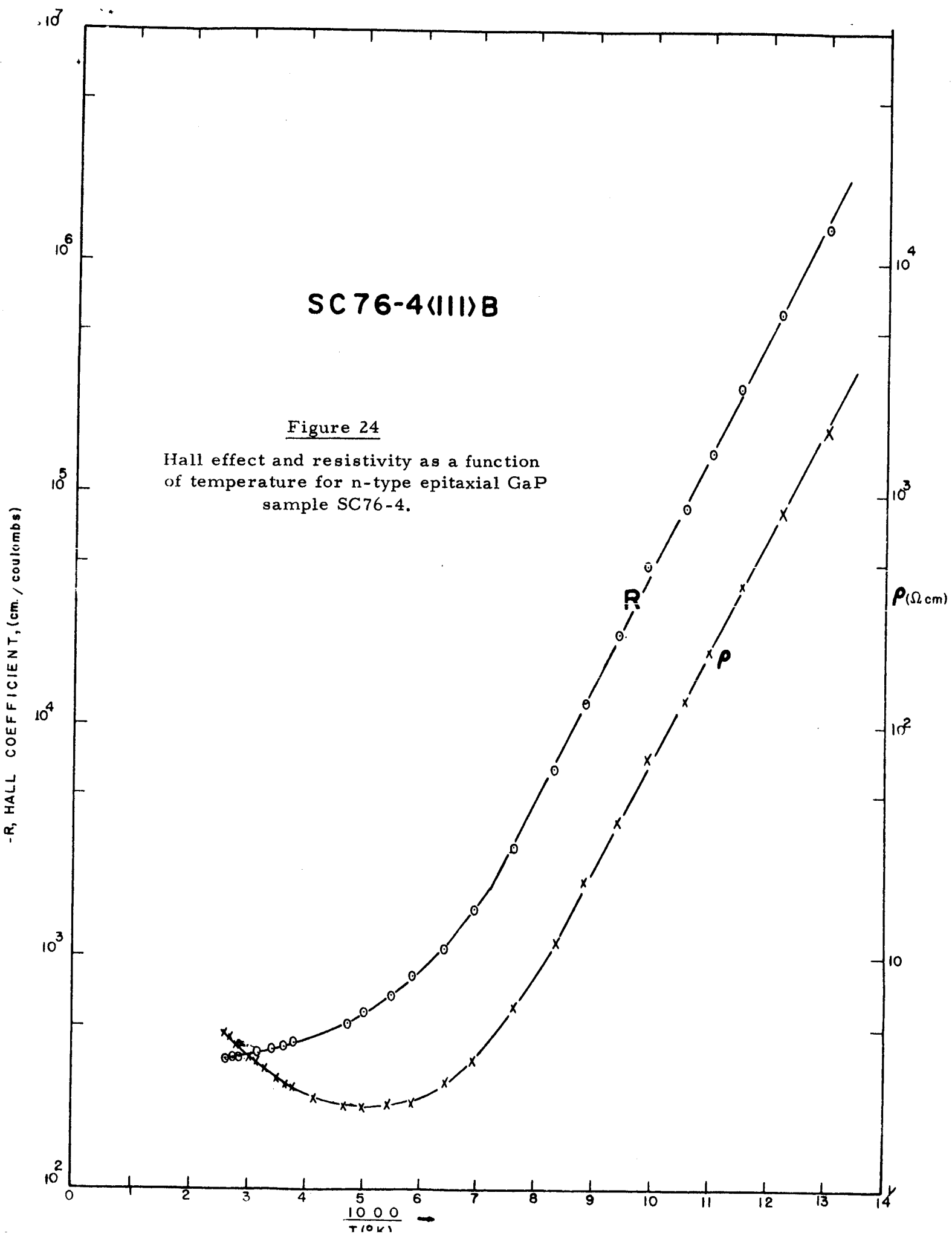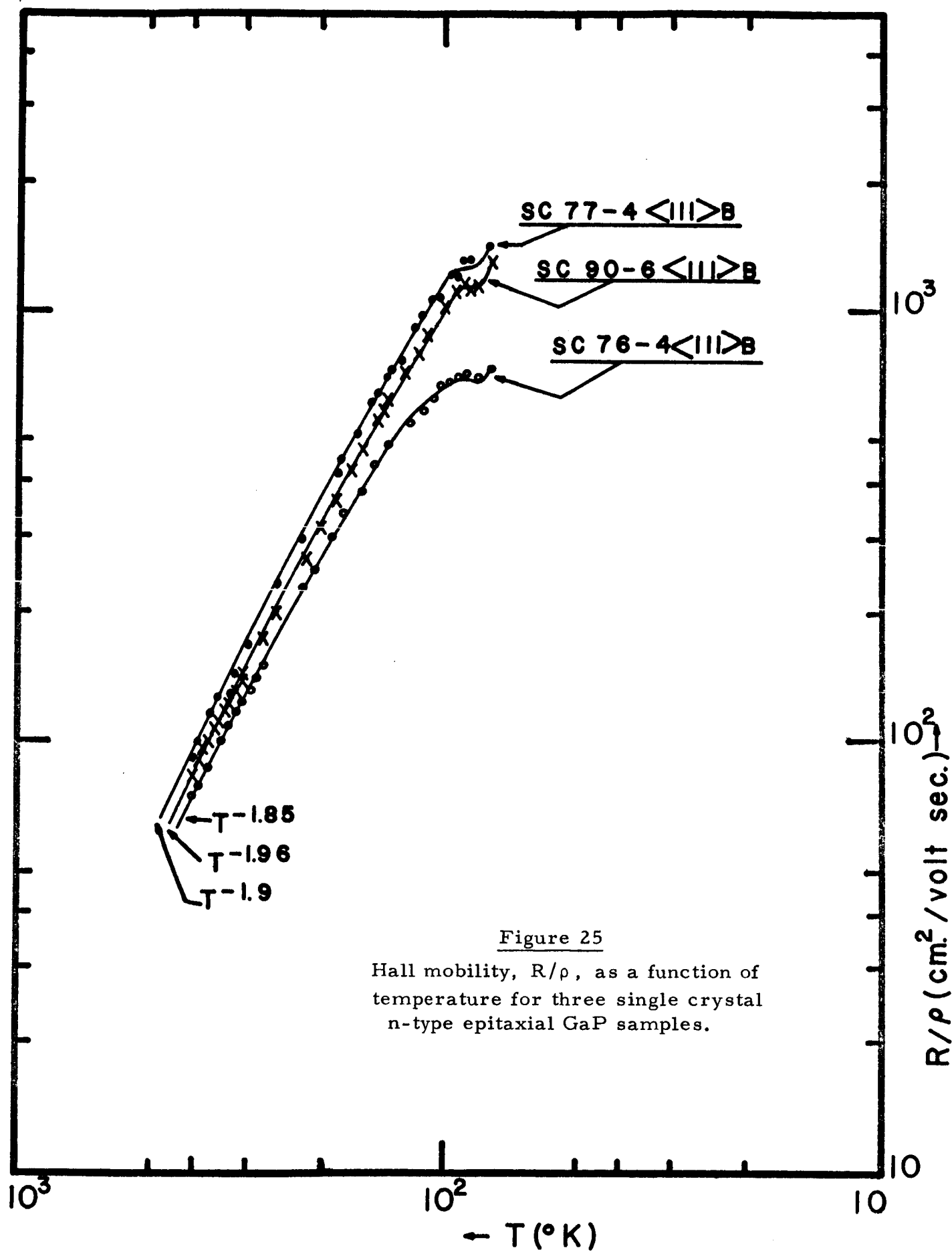
Figure 25

Hall mobility, R/ρ, as a function of temperature for three single crystal n-type epitaxial GaP samples.

DISTRIBUTION LIST

DISTRIBUTION LIST

DISTRIBUTION LIST

DISTRIBUTION LIST

No. of Copies

Bell and Howell Research Center
360 Sierre Madre Villa
Pasadena, California
Attn: Alan G. Richards   1

Bell Telephone Laboratories
Murray Hill, New Jersey
Attn: W. L. Brown   1
             U. B. Thomas   1

Clevite Research Center
540 East 105th Street
Cleveland, Ohio, 44108
Attn: F. A. Shirlend   1

The Eagle-Picher Company
Chemical and Material Division
Miami Research Laboratories
200 Ninth Avenue, N. E.
Miami, Oklahoma
Attn: John R. Musgrave   1

Harshaw Chemical Company
Solid-State Division
2240 Prospect Avenue
Cleveland, Ohio, 44115
Attn: James C. Schaefer   1

Heliotek Corporation
12500 Gladstone Avenue
Sylmar, California
Attn: Eugene Ralph   1

Hughes Aircraft Company
Aerospace Group, R and D Division
Culver City, California
Attn: C. A. Escoffery   1

Leesona Moos Laboratories
90-29 Van Wyck Expressway
Jamaica 18, New York
Attn: Stanley Wallack   1

DISTRIBUTION LIST

National Cash Register Company
Physical Research Department
Dayton 9, Ohio
Attn: R. R. Chamberlin   1

North American Aviation, Inc.
Autonetics Division
Anaheim, California
Attn: R. R. August   1

Philco Corporation
Blue Bell, Pennsylvania
Attn: Mr. A. E. Mace   1

Radio Corporation of America
RCA Research Laboratories
Princeton, New Jersey
Attn: P. Rappaport   1

Sandia Corporation
Albuquerque, New Mexico
Attn: F. Smits   1

Stanford University
Solid-State Electronics Laboratory
Stanford Electronics Laboratory
Stanford, California
Attn: Prof. G. L. Pearson   1

Westinghouse Electric Corporation
Research and Development Laboratories
Churchill Borough, Pennsylvania
Attn: H. C. Chang   1

Westinghouse Electric Corporation
Semiconductor Division
Youngwood, Pennsylvania
Attn: Don Gunther   1

DISTIBUTION LIST

No. of Copies

Massachusetts Institute of Technology   1
Semiconductor Division
Room 14-0641
Cambridge 39, Massachusetts

Tyco Laboratories, Inc.
Bear Hill
Waltham 54, Massachusetts
Attn: A. I. Mlavsky   1